RICE UNIVERSITY

Simulations of Adsorption and In-plane Ordering of Electrostatically Adsorbed Charged Colloidal Nanoparticles

by

Jennifer A Luna Singh

A THESIS SUBMITTED
IN PARTIAL FULFILLMENT OF THE
REQUIREMENTS FOR THE DEGREE

Doctor of Philosophy

APPROVED, THESIS COMMITTEE

Dr. Enrique Barrera, Thesis Director
Professor of Materials Science and NanoEngineering

Dr. Yildiz Bayazitoglu, Chair
Harry S. Cameron Chair Professor in Mechanical Engineering

Dr. Satish Nagarajaiah
Professor of Civil and Mechanical Engineering

Dr. Richard Vaia
Technical Director, Functional Materials Division, Materials and Manufacturing Directorate, Air Force Research Laboratory

HOUSTON, TEXAS
January 2016

ABSTRACT

Simulations of Adsorption and In-plane Ordering of Electrostatically Adsorbed Charged Colloidal Nanoparticles

by

Jennifer A Luna Singh

Self-limiting assembly of nanoparticle arrays promises to revolutionize compliant device fabrication by enabling print-on-demand. Presently, quantitative understanding of the relationship between the array order, nanoparticle size, nanoparticle interactions, surface characteristics, and process conditions remain elusive. Previous simulations have shown that tuning particle and surface potentials, screening lengths, and particle concentrations can lead to ordering. However, identifying the experimental conditions to observe these in-plane order-disorder and order-order transitions for nanoparticles remains a challenge. This study focuses on the ordering process during absorption of electrostatically stabilized nanoparticles onto an attractive surface with varying bulk concentrations of the nanoparticles in solution. The bond orientational correlation function as well as Voronoi and 2D structure factor analysis is used to determine the transition points between liquid, hexatic, and crystalline nanoparticle arrays. To better understand the role of hydrodynamic interactions between the particles simulations using Fast Lubrication dynamics were compared to the Brownian dynamics simulations. Both Brownian dynamics and Fast Lubrication dynamics simulations demonstrated that the critical effective surface coverage required for the liquid-hexatic or hexatic-crystalline transition point increases with increasing bulk concentration, while the critical timestep decreases with increasing bulk concentration. The computational cost of Fast Lubrication dynamics is approximately an order of magnitude greater than that of Brownian dynamics. The inclusion of particle-particle hydrodynamic interactions revealed a reduced bulk diffusion coefficient and the stochastic nature of the ordering process. Identifying and understanding these transition points will help elucidate experimental conditions necessary to create high resolution patterns and smaller devices.

Acknowledgments

Imagining something may be the first step in making it happen, but it takes the real time and real efforts of real people to learn things, make things, turn thoughts into deeds or visions into inventions. – Fred Rogers [1]

It has taken a lot of people's real time, effort, and support to make this thesis come to fruition. To my thesis advisor Dr. Enrique Barrera and my committee members Dr. Yildiz Bayazitoglu, Dr. Satish Nagarajaiah, and Dr. Richard Vaia, thank you for your continued support and sticking it out with me all these years. I'd like to thank the past and present members of Dr. Barrera's group especially Laura Peña-Parás and Jonathan Lee. Your friendship, hours of laughter, and knowledge have been instrumental to my success. I'd also like to thank the many staff members at Rice who have helped me along my journey especially Gary Cisneros, Maria Maldonado, Sherry Vanderslice, and Theresa Chatman. I am incredibly grateful for your positive spirit and continual help throughout my graduate work.

I am incredibly grateful for the experience and mentors I gained during my coop at the Air Force Research Laboratory, especially Dr. Richard Vaia, Dr. Vikas Varshney, and Dr. Katie Thorp. I'd like to thank everyone in the Materials and Manufacturing Directorate who welcomed me and shared their immense knowledge!

To my very large extended family, past teachers, and many friends who have been supportive over the years, thank you. I wouldn't have made it this far without all of your encouragement.

I don't have words to express the gratitude I have for the four incredible women I was forced to say goodbye to while in graduate school: Tamara Higgins, Marilyn Gold, Viola Luna, and Maria Venarske. You've left me with incredible life lessons and memories. I wish I could share this milestone with each of you.

Saving the best for last, I'd like to thank my Mom, Dad, and husband, Sameer. You are the best cheerleaders and I wouldn't be here without your unconditional love and support.

Table of Contents

List of Figures

List of Tables

Chapter 1

Introduction

1.1. Motivation

Many current applications are based upon assemblies of nano-objects which interact in purposeful ways. While small feature sizes are possible using techniques such as E-beam and nanoimprint lithography printing, cost and scalability are primary obstacles to engineering these surfaces. The challenge to develop facile, efficient and robust ways of mass assembling ordered nanostructures still exists. Potential uses in industries such as optics, photovoltaics, and sensors drive the need for better insight into the fundamental science driving these self-assembly methods. Bottom up self-assembly methods have the potential to produce simple, inexpensive, and reproducible nanoarrays. Basic understanding of nanoparticle adsorption and ordering can elucidate

experimental conditions necessary to create high resolution patterns and smaller devices. This study focuses on how structure evolves in electrostatic nanoparticle self-assembly from stable colloidal solution.

1.2. Background

1.2.1. Adsorption

Several different approaches have been used to model the adsorption and ordering of colloidal particles. Random sequential adsorption and 2D Lattice–based Monte Carlo simulations both determine equilibrium surface structures without including bulk effects. Random sequential adsorption is a simple model in which a single particle attempts to randomly adsorb onto a surface. If the particle does not overlap previously adsorbed particles, the particle adsorbs. Otherwise, the particle's adsorption is rejected and a new randomly selected position is attempted. Adsorption attempts occur until particles are unable to adsorb [2], [3]. While the random sequential adsorption model has been expanded to incorporate electrostatic interactions [4], hydrodynamics [5], particle tethering [6], polydispersity [7], patterned surfaces [8], it has significant limitations that prevent investigation of the adsorption and ordering process. The lack of in-plane surface diffusion prevents ordering from occurring, and as previously mentioned, usually no bulk effects are considered. Particles are adsorbed individually limiting analysis of the adsorption process. Similarly, 2D Lattice–based Monte Carlo

simulations only predict the equilibrium surface structure, but in contrast to random sequential adsorption, allow for in-plane diffusion. Of most interest, Monte Carlo simulations have been used to study the adsorption of particles with a hard core and soft shell potentials resulting in unique equilibrium surface structures such as stripes and clusters [9]–[12]. Like random sequential adsorption, however, these 2D Monte Carlo simulations do not include any bulk-effects and the ordering process cannot be examined.

Brownian Dynamics Simulation have been studied allowing for the analysis of the adsorption and ordering process [13]–[17]. This method captures the effects of the physical parameters of the system such as electrostatic, van der Waals, and Brownian forces. Further details of the governing equations used for Brownian Dynamics Simulations of adsorption of electrostatically stabilized nanoparticles onto an attractive surface are Given in section 2.1.

Oberholzer et al. developed a technique using grand canonical Monte Carlo reservoir and Brownian dynamics simulation box to maintain constant bulk concentration to study the adsorption process, but surface structures were not analyzed [13]. Gray and Bonnecaze used an open boundary cell technique and studied the effects of varying particle potentials, surface potentials, bulk concentrations, and Debye screening lengths determining that the final surface coverage and structure are almost independently controlled by wall potential and particle potential, respectively [14]. Miyahara et al. used a similar Brownian

Dynamics technique while varying the bulk concentration and Debye screening length in order to analyze the last adsorption process before an ordered state is formed. They determined that the mechanism for order formation is what they called the “one-directional average force”, which is further discussed in subsequent chapters [15]–[17].

Brownian Dynamics Simulations have been expanded to include bi -and poly-dispersity [18], [19], patterned surfaces [19], and friction [20]. Nonetheless, the surface size limitations of previous work have prevented determination of the liquid-hexatic and hexatic-crystalline transition points. This study expands the Brownian Dynamics simulation method to large scales in order to fully analyze the disorder-order transitions.

1.2.2. Hydrodynamics

Simulation techniques for colloidal suspensions including hydrodynamic interactions can be grouped into 2 categories: the fluid particles are explicitly considered or the fluid is treated as a continuum. Methods using explicit solvents include molecular dynamics, dissipative particle dynamics [21] and lattice Boltzmann methods [22]. Methods treating the fluid as a continuum include Brownian Dynamics with hydrodynamic interactions [23], and modern Stokesian Dynamics algorithms [24], [25]. These methods are far too computationally intensive to complete 3D simulations of the adsorption and ordering of electrostatically stabilized nanoparticles onto an attractive surface for the time

and length-scale required. Kumar and Higdon, recently developed a modified version of the Stokesian dynamics technique known as Fast Lubrication Dynamics with refinements required for long-time scale simulations. making the inclusion of bulk hydrodynamic interactions viable [26], [27].

Chapter 2

Computational Approach

The system studied consists of repulsive spherical particles in an aqueous medium adsorbing onto a highly attractive surface. In order to study the surface's structure evolution, both large length and time scales are required. Traditional molecular dynamic methods using explicit solvents are currently computationally impractical for simulations of this size. Monte Carlo methods are computationally efficient, but don't allow for dynamic understanding of the adsorption and ordering process. Thus a tradeoff between the systems complexity and computational expense is necessary.

2.1. Brownian dynamics

Brownian dynamics is a simulation method, which defines the motion of particles with an implicit solvent. It is a simplified Langevin dynamics without inertia. The force balance for all particles is

$$m\frac{dv}{dt} = F_C + F_F + F_R$$

where F_C is the conservative force (particle-particle and particle-surface potentials), F_F is the viscous drag term , and F_R is a random force due to the solvent bumping into the particle at a given temperature. The random force is not linked to any surrounding particles or the presence of a wall, so momentum is not conserved and hydrodynamic interactions are neglected. A Langevin thermostat with NVE integration is used in LAMMPS to perform Brownian dynamics [28]–[30].

2.1.1. Interaction Potentials

Particle-particle and particle-surface interactions are modeled using DLVO theory composed of electrostatic and van der Waals interactions. The repulsive electrostatic double-layer potentials for particle-particle (pp) interactions and attractive particle-surface interactions (ps) are

$$E_{pp} = \frac{A}{\kappa}e^{-\kappa(r-2a)}, \qquad A = \kappa\left(\frac{a}{2}\right)Z$$

$$E_{ps} = aZe^{-\kappa D}, \qquad Z = 64\pi\varepsilon_0\varepsilon\left(\frac{kT}{e}\right)^2 \tanh^2\left(\frac{ze\psi_0}{4kT}\right)$$

where a is the particle's radius, r is the distance between particle centers, D is the distance between the surface and the particle's surface, κ is the inverse screening length, z is the valency of the ion, ε_0 is the vacuum permittivity, ε is the relative permittivity, e is the elementary charge, k is the Boltzmann's constant, T is the temperature, and ψ_0 is the surface potential [31], [29], [32], [13], [33].

The Van der Waals attraction and hard core repulsion potentials for particle-particle (pp) interactions and particle-surface interactions (ps) are

$$U_{pp} = U_A + U_R$$

$$U_A = -\frac{A_{pp}}{6}\left[\frac{2a^2}{r^2-4a^2} + \frac{2a^2}{r^2} + \ln\left(\frac{r^2-4a^2}{r^2}\right)\right]$$

$$U_R = \frac{A_{pp}}{37800}\frac{\sigma^6}{r}\left[\frac{r^2-14ra+54a^2}{(r-2a)^7} + \frac{r^2+14ra+54a^2}{(r+2a)^7} - 2\left(\frac{r^2-30a^2}{r^7}\right)\right]$$

$$U_{ps} = A_{ps}\left[\frac{\sigma^6}{7560}\left(\frac{6a-D}{D^7} + \frac{D+8a}{(D+2a)^7}\right)\right.$$

$$\left. -\frac{1}{6}\left(\frac{2R(D+a) + D(D+2a)[\ln D - \ln(D+2a)]}{D(D+2a)}\right)\right]$$

where a is the particle's radius, r is the distance between particle centers, D is the distance between the surface and the particle's surface, σ is the size of constituent LJ particle, and A_{pp} and A_{ps} are Hamaker's constants.

It should be noted that these interaction potentials are only valid for systems where $\kappa a > 1$. Physical parameters used in these simulations for polystyrene latex spherical particles in an aqueous solution are given in Table 2.1 and the particle-particle and particle-surface interactions are shown in Figure 2.1 and 2.2, respectively. The inverse screening length, surface potential, and other values given in Table 2.1 were chosen to represent a realistic experimental systems [31].

Table 2.1 – Physical Parameters

Particle radius, a (nm)	50
Volume fraction, ϕ	0.05 - 0.11
Inverse screening length, κ (m^{-1})	$1x10^{-8}$
Temperature, T (K)	298
Relative permittivity, ε	80
Surface potential, ψ_0 (V)	0.137
Hamaker constant, A_{pp} (J)	$95x10^{-20}$
Hamaker constant, A_{ps} (J)	$1.60x10^{-20}$

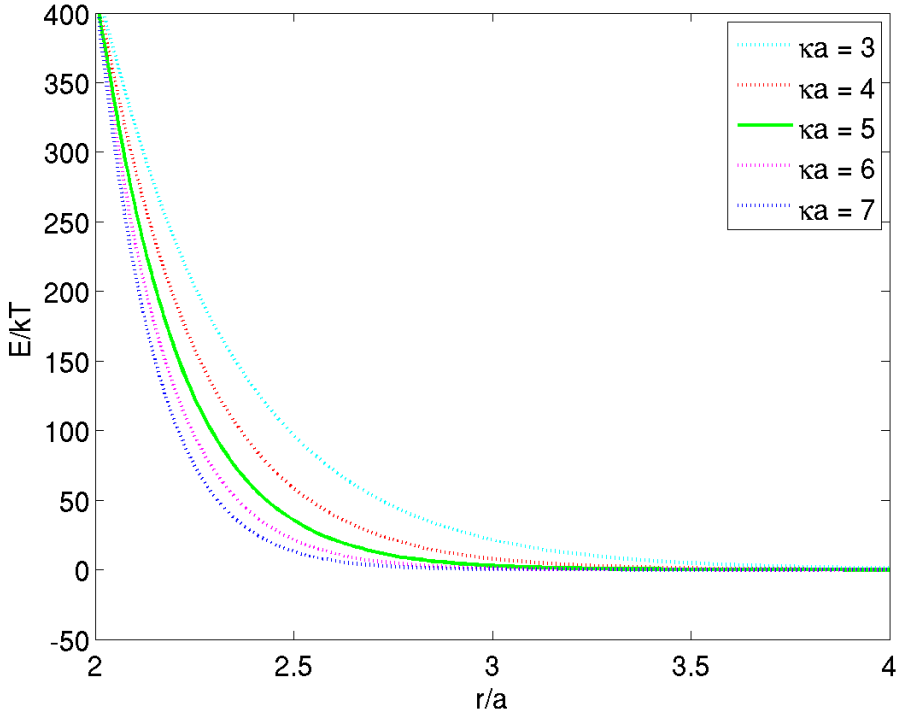

Figure 2.1 – Particle-Particle Potential

2.1.1. Simulation Setup

Great care was taken to confirm the results presented are a result of the kinetics of the system and not an artifact of the simulation setup. In order to ensure that the box size and initial particle placement did not influence the ordering process, the simulation setups shown in Table 2.2 were tested for varying bulk concentrations. It was important to have a simulation box that mimics experimental conditions with uniform bulk concentration throughout the adsorption process and boundary conditions that do not influence the ordering process.

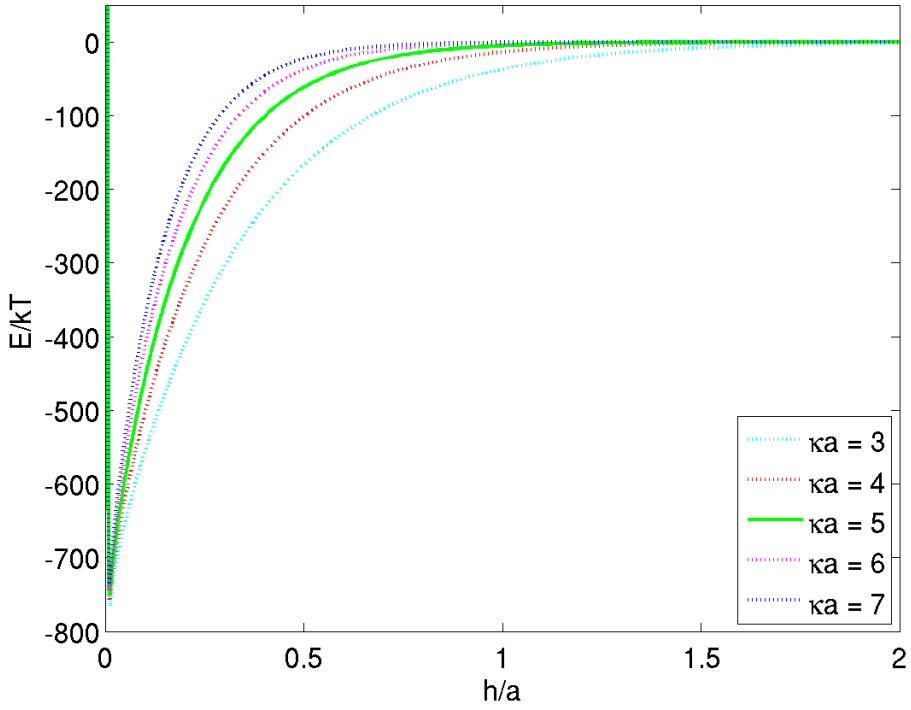

Figure 2.2 – Particle-Surface Potential

In order to maintain constant bulk concentration and hence constant chemical potential, 2 methods were tested. The first method is to have a very tall box such that the maximum number of adsorbed particles is about 2% of the total number of particles, thus reducing the bulk concentration negligibly. A very tall box also ensures that any particle density fluctuation or effects from the upper boundary do not affect adsorption or ordering on the surface. For large bulk concentrations, a very tall box height is $200a$. This method ensures that the simulation's top boundary condition does not effect adsorption, but requires large computation expense due to the large

Table 2.2 – Simulation Setups

	Box Height			Additional Particles	Equilibrium Method				Gap Space		
	200a	100a	50a		None	Periodic Boundary	Reflecting z Boundary	LAMMPS Minimize	0	a	4a
A	x							x	x		
B	x					x					x
C	x			x		x					x
D	x						x			x	
E	x			x			x			x	
F			x	x		x				x	
G			x	x		x					x
H			x	x	x				x		
I			x	x			x			x	
J		x		x		x				x	
K		x		x		x					x
L		x		x	x				x		
M		x		x			x			x	

number of particles in the system. This method also becomes impractical at small bulk concentrations, since the size of the simulation box would need to increase dramatically to ensure only 2% of the bulk adsorbs onto the surface.

The second method is to determine an appropriate box height based on the maximum depletion length and the bulk diffusion coefficient. The maximum depletion length was determined by analyzing the density fluctuations in the bulk during adsorption due to the charged surface. The necessary box height needs to be greater than the maximum depletion length plus the average distance traveled by a particle in the bulk to reach the surface. This ensures that any particle density fluctuation or effects from the upper boundary does not affect

adsorption or ordering on the surface. To keep a constant concentration, particles need to be added to the bulk as particles are adsorbed. Particle density fluctuations near the surface and bulk diffusion coefficient depend on the bulk concentration. Conservatively, the necessary box height was determined to be $100a$ for bulk concentrations less than 0.08 and $50a$ for bulk concentrations greater than 0.08. For large bulk concentrations considered in this study, this method can save considerable computational time by reducing the system size to ¼ or ½ of the required size using the tall box method. Several small scale simulations using both methods were completed to confirm proper box height was determined for each bulk concentration. Using an appropriate box height, the two methods showed no significant difference is adsorption rate or phase transition point.

Several methods for determining initial particle placement were tested including random placement of particles with no equilibrating process, random placement of particles using LAMMPS minimize command, random placement of particles equilibrated for 10^6 steps with periodic boundary conditions in the x and y directions and reflecting boundary conditions in the z direction, and random placement of particles equilibrated for 10^6 steps with periodic boundary conditions in all directions. In addition, the bottom z boundary was increased by a gap space when periodic or reflecting boundary conditions were used in the z direction. A gap space of minimum than length a ensured that particles were not overlapping the surface and a gap space of length $4a$ ensured no particles were

initially on the surface. Short-time adsorption curves for the simulation setups A-I in Table 2.2 for a simulation with bulk concentration of 0.11 are presented in Figure 2.3. It was found that the initial particle placement greatly affected the initial adsorption rate, but all of the initial simulation set-ups converged around 10^8 steps and the initial adsorption rate had no effect on the final adsorption or phase transition points.

Since the work presented here focuses on the phase transition point, which all occur well after 10^8 timesteps, the most computationally efficient setup

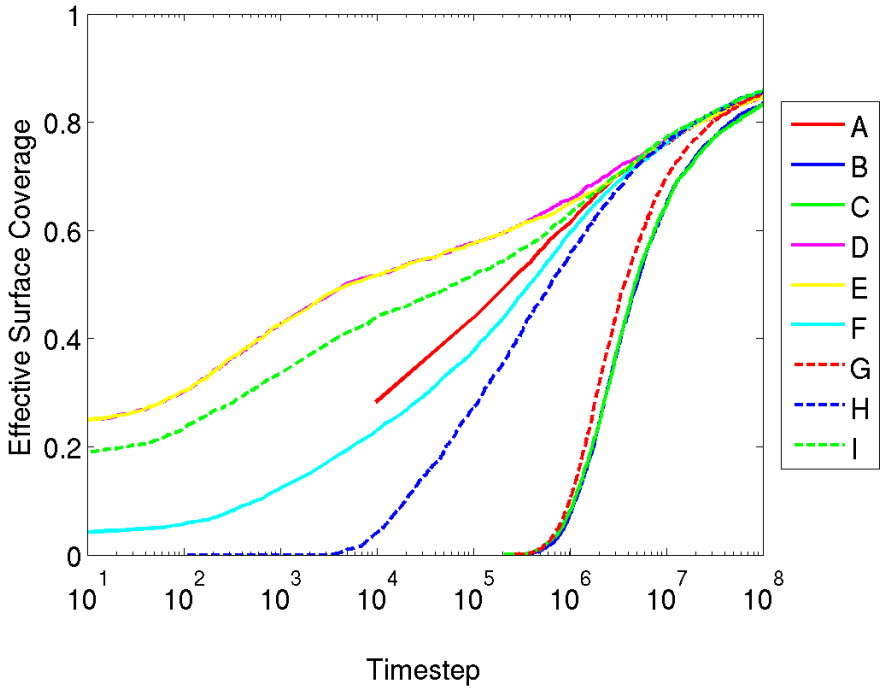

Figure 2.3 – Short-time adsorption curves for simulation setups A–I in Table 2.2 for Brownian dynamics simulations with bulk concentration of 0.11

was chosen to complete multiple simulations for full analysis. All results presented in the following chapters will have a reduced simulation box height based on bulk concentration with additional particles added as adsorption occurs and the initial particle placement will be determined from random placement of particles equilibrated for 10^6 steps with periodic boundary conditions in all directions and a gap space of length a. A box length and width of $150a$ is used to ensure sufficient particles adsorb on the surface for statistical analysis as order correlation functions require approximately 2000 particles on the surface to be accurately determined [34].

2.1.2. Simulation Procedure

Particles are randomly placed inside the box such that they are a minimum of $2.2a$ away from one another. The particles are equilibrated in the box for 10^6 steps with periodic boundary conditions in all directions using a timestep of 0.03 (3.43×10^{-10} s). The bottom z boundary is increased by length a and made a fixed wall with the above mentioned potential. The top z boundary is set as reflecting and the x and y boundaries remain periodic. The system is run for 3×10^5 steps with a timestep of 0.001 (1.14×10^{-11} s) to ensure particles close to the charged surface do not overlap as initial adsorption occurs. The system is then run at a timestep of 0.03 (3.43×10^{-10} s) for the remainder of the simulation. Once a particle's center point is at a distance $1.1a$ from the surface, it is considered adsorbed. To maintain bulk concentration, new particles are added to

the top region of the simulation box a maximum distance of $3a$ from the top boundary every 10^3 steps in the same quantity as adsorbed. Each system was run 3 times with different initial random particle placements. Due to the computational time required for low bulk concentrations to adsorb and order, only bulk concentrations greater than 0.04 are studied. A schematic of the procedure and simulation box set-up is shown in Figure 2.4.

2.1.3. Assumptions

The Brownian dynamics simulation described includes several important assumptions. As previously mentioned, the fluid is assumed to be still and hydrodynamic interactions are ignored. It is also assumed that no gravity is present. The surface is assumed to be frictionless.

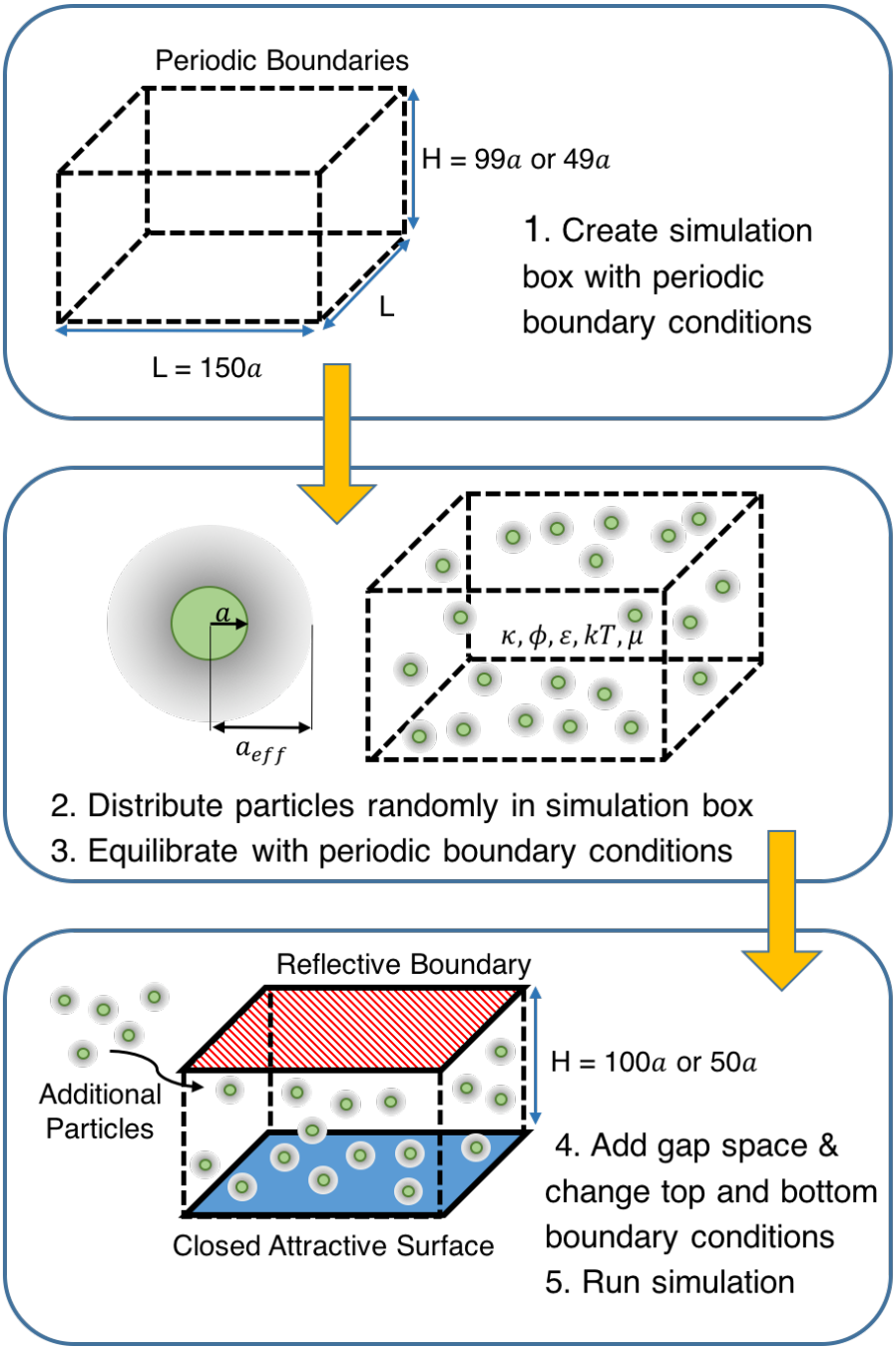

Figure 2.4 – Schematic of Brownian dynamics simulation procedure

2.2. Fast Lubrication dynamics

The Fast Lubrication dynamics are incorporated in LAMMPS as pairwise hydrodynamic interactions between mono-disperse spherical particles with 2 components. The first component is the Ball-Melrose lubrication terms via the formulas derived in Ball and Melrose describing the general expression for the dissipation, *W,* of a pair of close spheres by transforming to the corotating and cotranslating frame of the pair treated as a dumbbell [35]

$$W = -a_{sq}|(\mathbf{v}_1 - \mathbf{v_2}) \cdot \mathbf{nn}|^2 - a_{sh}|(\omega_1 + \omega_2) \cdot (\mathbf{I} - \mathbf{nn}) - 2\Omega_N|^2$$
$$-a_{pu}|(\omega_1 - \omega_2) \cdot (\mathbf{I} - \mathbf{nn})|^2 - a_{tw}|(\omega_1 - \omega_2) \cdot \mathrm{nn}|^2$$

$$\Omega_N = \mathrm{n} \times (\mathbf{v}_1 - \mathbf{v_2})/r$$

where $\mathbf{v}_1$, and $\mathbf{v}_2$ are the translational velocities, ω_1, and ω_2 are the angular rotations, $\mathbf{r} = r\mathbf{n}$ is the center the center vector between particle, and the angular rotation if the dumbbell is divided into four components: squeeze, shear, pump, and twist [36], [37].

The second component consists of the Fast Lubrication dynamics approximation derived by Kumar and Higdon to balance forces and torques, F^H [26], [27]

$$F^H = -R_{FU}(U - U^\infty) + R_{FE}E^\infty$$

where U represents the velocities and angular velocities of the particles, U^∞ represents the velocity and angular velocities of the undisturbed fluid, E^∞

represents the rate of strain tensor of the undisturbed fluid with a given kinematic viscosity, R_{FU} denotes the component of the resistance tensor representing the generalized force-velocity coupling, and R_{FE} denotes the generalized force and rate of strain tensor coupling.

2.2.1. Simulation Setup

Implementing Fast Lubrication dynamics necessitate a certain simulation setup. Volume fraction calculations prohibit the addition of particles, so a large box size is required to maintain constant bulk concentration. In addition, the implementation of Fast Lubrication dynamics in LAMMPS does not allow for a reflecting boundary on the top z boundary. To prevent particles from escaping from the box or pooling at the top surface, a repulsive potential was added to the top boundary. Therefore, the Fast Lubrication dynamics results presented in the following chapters will have a simulation box height of $200\,a$ and the initial particle placement will be determined from random placement of particles equilibrated with periodic boundary conditions in all directions and a gap space of length a. A box length and width of $150\,a$ is used to ensure sufficient particles adsorb on the surface for statistical analysis as order correlation functions require approximately 2000 particles on the surface to be accurately determined .

2.2.2. Computational Cost

Fast Lubrication dynamics are computationally efficient compared to other methods of incorporating hydrodynamic interactions. The addition of hydrodynamics as well as the required simulation setup, however, significantly increases the computational cost of these simulations when compared to Brownian dynamics simulations. The estimated computational cost of Fast Lubrication dynamics can be compared to that of Brownian dynamics as shown in Table 2.3.

Table 2.3 – Computaional cost of Fast Lubrication dynamics compared to Brownian dynamics simulations

	Brownian dynamics	Fast Lubrication dynamics
Timestep	0.03 (3.43×10^{-10} s)	0.01 (1.14×10^{-10} s)
Real Time to complete a timestep (based on ppp conditions)	t_{step}	1.3 t_{step}
Constant ϕ Method	Small Box with Additional Particles	Big Box
Box Height	For ϕ=0.07: H=100a For ϕ= 0.09: H=50a	H=200a
Top Boundary Condition	Reflecting	Repulsive
Estimated Real Time to complete simulation	t	For ϕ=0.07: 7.8 t For ϕ= 0.09: 15.6 t

The required timestep for Fast Lubrication dynamics is a third of that used for the Brownian dynamics solutions. Small scale simulations with all periodic boundary conditions were used to determine the approximate real time required to complete a timestep, which was determined to be approximately 1.3 times the that required to complete a Brownian dynamics timestep. Due to the required large box size, there are 2 to 4 times more particles in the system depending on the bulk concentration. Thus, assuming that these additions affect the computational cost linearly, the estimated real clock time to complete a Fast Lubrication dynamics simulation is 7.8 or15.6 times longer that for a Brownian dynamics simulation for bulk concentrations of 0.07 and 0.09, respectively. This estimation is a best case scenario given that this estimation was based on small scale periodic simulations and does not include the increased computational cost due to the required repulsive top boundary. Given that the real time required to reach the hexatic-crystalline transition point for the Brownian dynamics simulations described using 256 processors with 16 cores each on a SGI ICE X or Cray XC30 system requires 1 to 3 weeks depending on the bulk concentration, the required real time and computational cost to compete a Fast Lubrication dynamics simulations is substantial on the order of 8 to 24 weeks and 330,000 to 1,000,000 cpu hours. Due to the large computational cost of Fast Lubrication dynamics, only a limited number of simulations were completed. Simulations for bulk concentrations 0.09, and 0.11 were run for 8 weeks (330,000 cpu hours), while simulations for a bulk concentration of 0.07 were run for 12 weeks (495,000

cpu hours). Two simulations at each bulk concentration were completed. Despite the shortcomings of the estimations, the real time required for large-scale simulations for both bulk concentrations was within 20% of the estimation. The estimation failed to account for the decreased diffusion coefficient observed in the Fast Lubrication dynamics, which is discussed in Chapter 4, so the hexatic-crystalline transition points for the simulation required more computational time than initially estimated.

2.2.3. Simulation Procedure

Particles are randomly placed inside the box such that they are a minimum of 2.2a away from one another. The particles are run in the box for $3x10^6$ steps with periodic boundary conditions in all directions using a timestep of 0.01 ($1.14x10^{-10}$ s) using Brownian dynamics to establish temperature in the system. Hydrodynamic interactions are then added to the system and the thermostat is modified to accommodate the Fast Lubrication dynamics while maintaining Brownian motion at a constant temperature. The particles are then equilibrated in the box for $3x10^6$ steps with periodic boundary conditions in all directions using a timestep of 0.01 ($1.14x10^{-10}$ s).The bottom z boundary is increased by length a and made a fixed wall with the same potential used in the Brownian dynamics simulations. The top z boundary is increased by length a and set as repulsive, while the x and y boundaries remain periodic. The system is then run at a timestep of 0.01 ($1.14x10^{-10}$ s) for the remainder of the simulation.

Once a particle's center point is at a distance $1.1a$ from the surface, it is considered adsorbed. Due to the large computational cost of these simulations, only 2 runs at bulk concentrations of 0.07, 0.09, and 0.11 were completed. A schematic of the procedure and simulation box set-up is shown in Figure 2.5.

2.2.4. Assumptions

Like the Brownian dynamics simulations, the Fast Lubrication dynamics simulation described assumes the fluid is considered still with no external flow present, no gravity is present, and the surface is assumed to be frictionless. Hydrodynamic interactions in the bulk and between particles on the surface are included, but hydrodynamic interactions between the surface and the particle are ignored due to the complexity of implementing the interactions into the simulations.

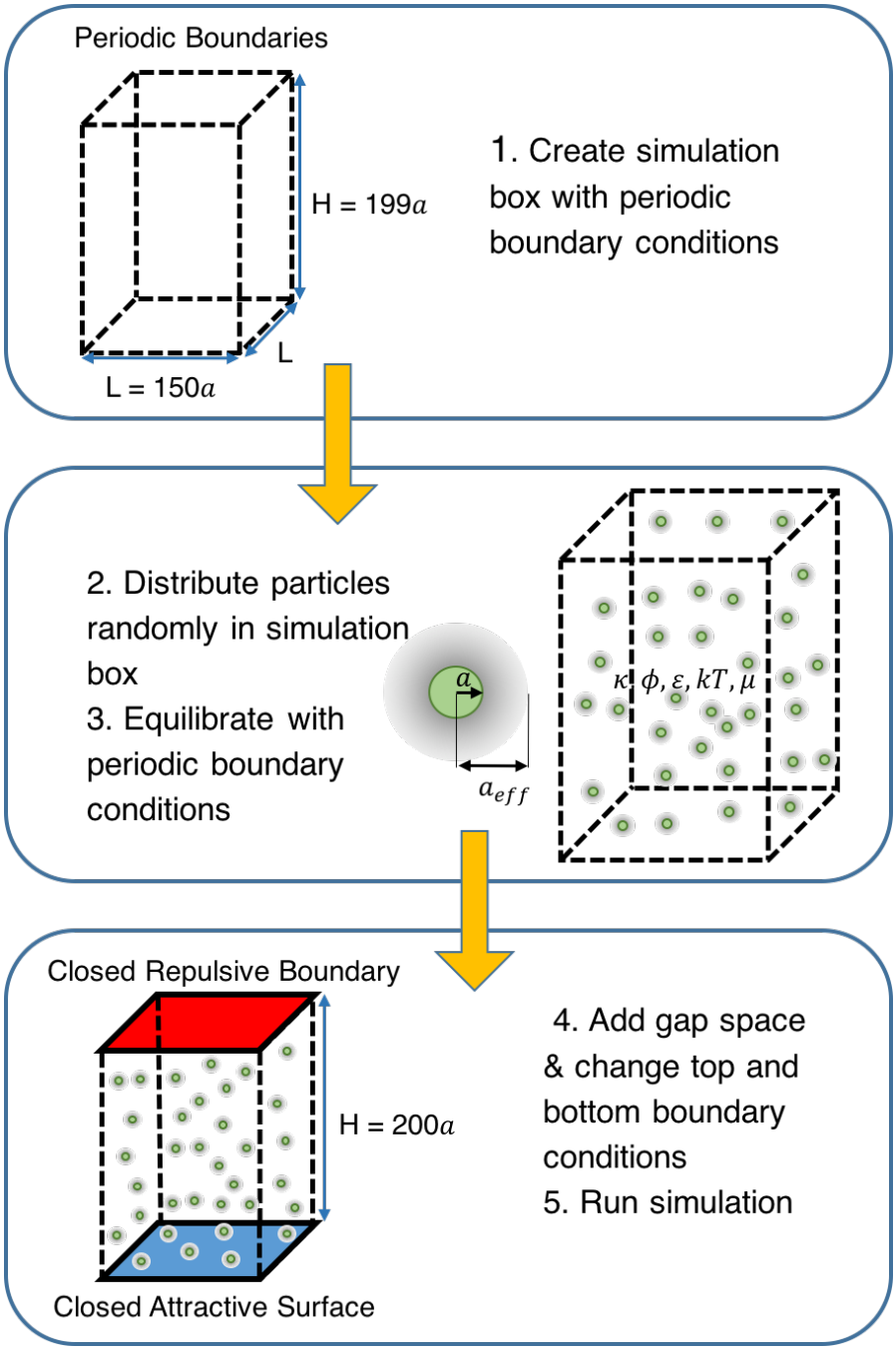

Figure 2.5 – Schematic of Fast Lubrication dynamics simulation procedure

2.3. Reduced Units

Lennard-Jones reduced units with $\sigma = 1nm$, $\varepsilon = kT = 4.12 \times 10^{-21} J$, and $m = 5.39 \times 10^{-16} g$ were used for all of the simulations. All quantities in the following chapters will be in reduced units unless otherwise noted and the asterisks notation has been omitted for simplicity.

Distance, $x^* = \frac{x}{\sigma}$ Energy, $E^* = \frac{E}{\varepsilon}$

Time, $t^* = t\left(\frac{\varepsilon}{m\sigma^2}\right)^{\frac{1}{2}}$ Force, $F^* = F\frac{\sigma}{\varepsilon}$

In addition, all timesteps presented in the following chapters have been normalized to a timestep of 0.03 (3.43×10^{-10} s). In an effort to easily extend the results presented to any systems of colloidal particles, the effective surface coverage rather than the surface coverage or number of adsorbed particles is presented.

Chapter 3

Analysis Methods

3.1. Voronoi

For a given set of points, a boundary can enclose each point such that any arbitrary point within the boundary is closer to the given point in the boundary than any other given point. The boundary is labeled a Voronoi polygon or cell and the collection of all the Voronoi cells constructs a Voronoi diagram. Voronoi diagrams can be used to visually characterize a systems ordered phase as well as show defect concentrations.

Voronoi cells for perfect 2D hexagonal crystals consist of regular hexagons. Real crystals' Voronoi cells will consist of hexagons, but will not be perfectly regular due to lattice fluctuations. As order decreases in the system, highly irregular hexagon cells as well as pentagons and heptagon will be present

representing defects. For the Voronoi diagrams presented in this work, cells are colored based on their shape to clearly identify defects. Hexagons are white, pentagons are pink, heptagons are green, and octagons are yellow. As shown in Figure 3.1, disclinations are represented as single non-hexagonal cells, free dislocations are characterized by paired pentagon and heptagon cells, and a dislocation pair consist of two combined free dislocations. A grain boundary is represented by a string of free dislocations. Voronoi diagrams for liquid phases are dominated by disclinations [38], [34], [39].

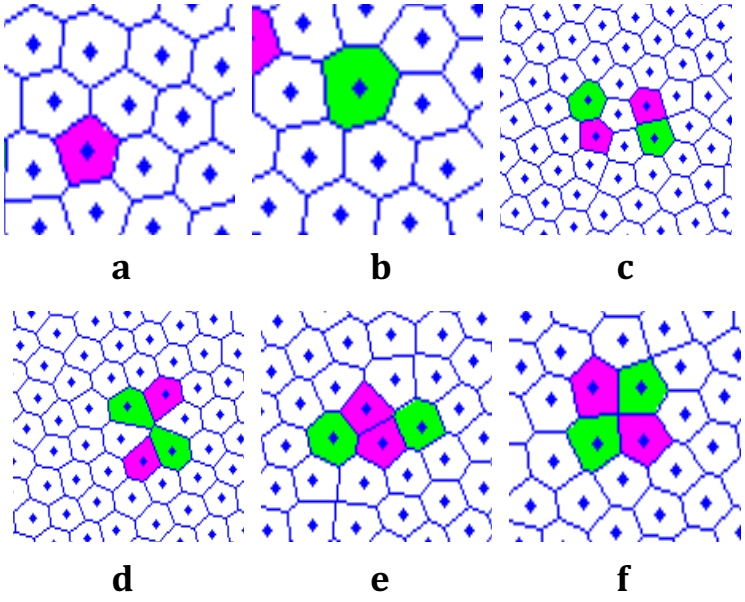

Figure 3.1 – Voronoi representation of defects. a & b: disclination, c: free dislocation, d & e: free dislocations in the process of binding or unbinding, f: dislocation pair

3.2. Bond Orientational Correlation Function

The bond orientational correlation function, $g_6(r)$, is a tool commonly used in melting theory to identify phase transitions defined as

$$g_6(r = |\boldsymbol{r}_k - \boldsymbol{r}_l|) = \langle \psi_6^*(\boldsymbol{r}_k)\psi_6(\boldsymbol{r}_l)\rangle$$

with the local six fold bond orientational parameter defined as

$$\psi_6(\boldsymbol{r}_k) = \frac{1}{n_l}\sum_{i=1}^{n_l} \mathrm{e}^{i6\theta_{kl}}$$

where n_l is the number of nearest neighbors to particle k and $\theta_{kl}$is the angle between particle k and particle l with respect to a fixed reference axis. The $\langle \quad \rangle$ brackets denote an ensemble average.

The bond orientational correlation function has a value between 0 and 1 for all r. The degree of order of a system can be characterized by the decay of $g_6(r)$. For a perfect 2D hexagonal crystal, $g_6(r) = 1$ and only exists at integer multiples of the lattice spacing reflecting long-range order. Real crystals, however, will have a value less than 1 due to lattice fluctuations. The quasi-long range ordered hexatic phase is characterized by an algebraic decay of $g_6(r)$ due to the existence of a small steady-state concentration of unbound dislocations. The evolution from algebraic decay to exponential decay marks the anisotropic hexatic to isotropic fluid phase transition. Free disclinations are present in short-range ordered liquid phase. By computing the bond orientational correlation

function as adsorption occurs, phase transition points can be defined [34], [39], [40].

3.3. 2D Structure Factor

Further confirmation of phase identification can be acquired from determining the structure factor as a function of time, defined as

$$S(\mathbf{q},t)=\frac{1}{N}\sum_{i=1}^{N}\sum_{j=1}^{N}\exp\left(i\mathbf{q}\boldsymbol{r}_i(\boldsymbol{t})\right)\exp\left(-i\mathbf{q}\boldsymbol{r}_j(t)\right)$$

The isotropic structure factor $S(q)$ is obtained through an angular average of the structure factor $S(\mathbf{q})$. Figure 3.2 shows examples of 2D structure factors corresponding to liquid, hexatic, and crystalline phases and their corresponding Voronoi diagrams with defects highlighted and bond orientational correlation functions. The structure factor for an isotropic liquid phase shows no defined peaks. The hexatic phase's structure factor exhibits six fold angular symmetry with widened, slightly diffused peaks. Sharp, well defined peaks with six fold angular symmetry characterize the crystalline phase. The structure factor alone is insufficient to determine phases or transitions points, but when combined with Voronoi diagrams and the bond orientational correlation function, the three tools provide sufficient verification for phase analysis and transition points[34], [40], [41].

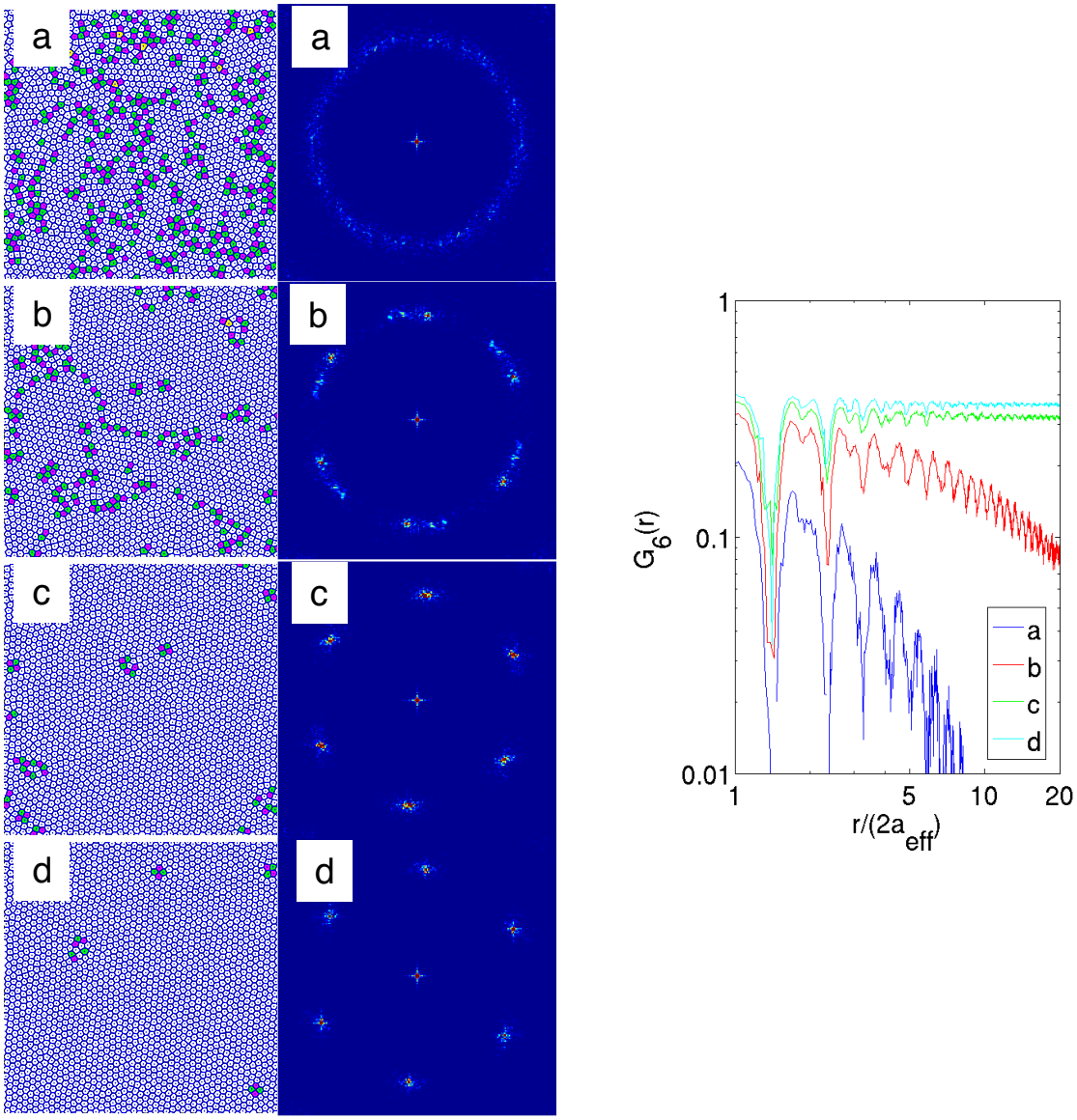

Figure 3.2 – Example Voronoi diagrams, 2D structure factors , and bond orientational correlation fuctions for the a) liquid phase, b) hexatic phase, and c & d) crystalline phase

Chapter 4

Simulations & Analysis

Brownian Dynamic simulations at bulk concentrations of 0.05, 0.07, 0.09, and 0.11 and Fast Lubrication dynamics simulations at bulk concentrations of 0.07, 0.09, and 0.11 are presented here. It should be noted that these concentrations are several orders of magnitude greater than those commonly used in experimental systems. Some previously published simulations were able to model systems with concentrations an order of magnitude lower than those presented here, but were far too small of systems to obtain statistical data for ordering analysis [14], [19]. While the lower bulk concentrations were still significantly greater than those used experimentally, they did allow the authors to analyze the early diffusion limited adsorption regime as well as the long time kinetically limited saturation regime. The time and length scales required for

lower bulk concentrations, make large simulation impractical at this time. The analysis presented here focuses on the kinetically limited regime[42]–[45].

4.1. Brownian dynamics Simulations

4.1.1. Adsorption

The adsorption curves for each of the Brownian dynamics simulations is shown in Figure 4.1. While this simulation does not prevent de-adsorption from occurring, no de-adsorption was expected or observed in any of the simulations and the adsorption process is essentially irreversible. The adsorption process matched previously published Brownian dynamics simulations of similar systems. Consistent with the results presented by Miyahara et al., the plateaued effective surface coverage obtained is dependent on bulk concentration due to the energy barrier created by the adsorbed particles on the surface preventing the adsorption of additional particles from the bulk [15]–[17]. Due to time constraints, these simulations were not run to equilibrium, but rather to the beginning of their plateau region. Given sufficient time, it is expected that adsorption would continue occur until all of the simulations resulted in crystalline adsorbed surfaces. Given infinite time, however, it is possible for the adsorption curves to converge to a closed packed surface regardless of the bulk concentrations.

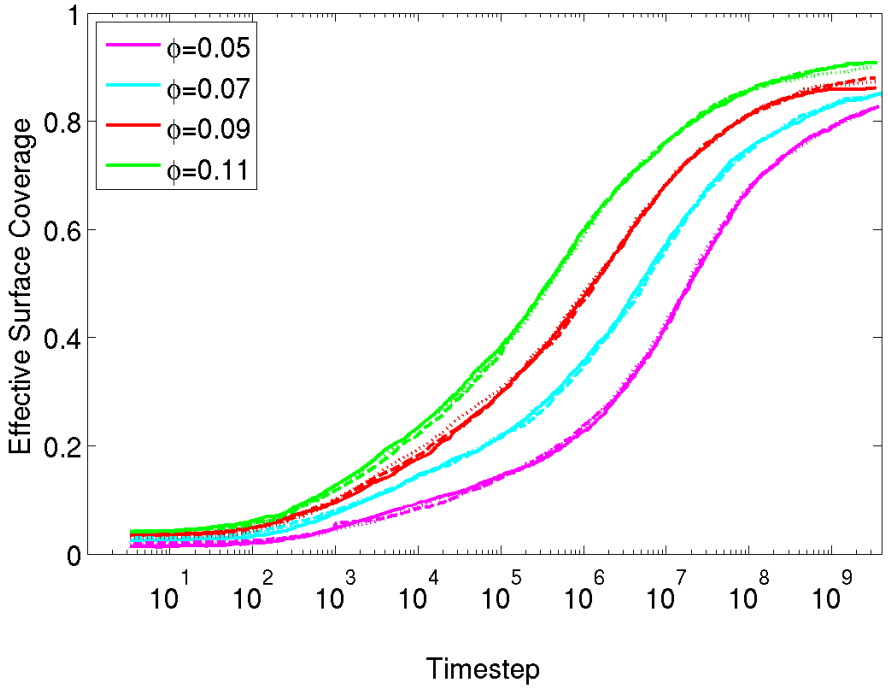

Figure 4.1 – Adsorption curves for Brownian Dynamic simulations with bulk concentrations of 0.05, 0.07, 0.09, and 0.11. For each bulk concetration, the 3 simulations performed with different intial random particle placement as dotted, dashed, and solid lines in the same color.

4.1.2. Ordering

For each of the Brownian dynamics simulations, the bond orientational correlation function was used to determine the liquid-hexatic and hexatic-crystalline transition point during the adsorption process. The exact number of particles adsorbed, n, and timestep at each transition point is given in Table 4.1. The averaged adsorption curve for each bulk concentration and averaged transition point for each bulk concentration is shown in Figure 4.2.

For colloidal particles, the jamming limit from random sequential adsorption models occurs at an effective surface coverage of 0.547. Using 3D hard sphere crystallization fraction the order-disorder transition has been estimated to occur at an effective surface coverage of 0.70 and a closed-packed surface occurs at an effective surface coverage of 0.9069 [29], [46], [14]. In many of the previous Brownian dynamics adsorption studies, the radial distribution function has been used to qualitatively determine an order-disorder transition point. In these simulations, a fixed surface coverage was assumed to be the order-disorder transition point for a given particle-particle and particle-surface

Table 4.1 – Transition points for Brownian Dynamic simulations with bulk concentrations of 0.05, 0.07, 0.09, and 0.11. For each bulk concetration, the 3 simulations performed with different intial random particle placement are represented as BD1, BD2, and BD3.

	Φ	LIQUID-HEXATIC		HEXATIC-CRYSTALLINE	
		n	Timestep	n	Timestep
BD 1	0.05	2040	2.7250E+09	not reached during simulation	
BD 2	0.05	2037	2.5500E+09	not reached during simulation	
BD 3	0.05	2050	3.4000E+09	not reached during simulation	
BD 1	0.07	2043	7.9500E+08	2079	1.4000E+09
BD 2	0.07	2059	8.8000E+08	2085	1.2500E+09
BD 3	0.07	2054	8.0000E+08	2085	1.4000E+09
BD 1	0.09	2083	2.3000E+08	2109	4.1000E+08
BD 2	0.09	2118	4.0000E+08	2135	6.0000E+08
BD3	0.09	2087	2.3000E+08	2135	4.5000E+08
BD 1	0.11	2134	1.0500E+08	2213	5.0000E+08
BD 2	0.11	2216	5.0000E+08	2223	5.8000E+08
BD 3	0.11	2136	1.0000E+08	2163	1.7000E+08

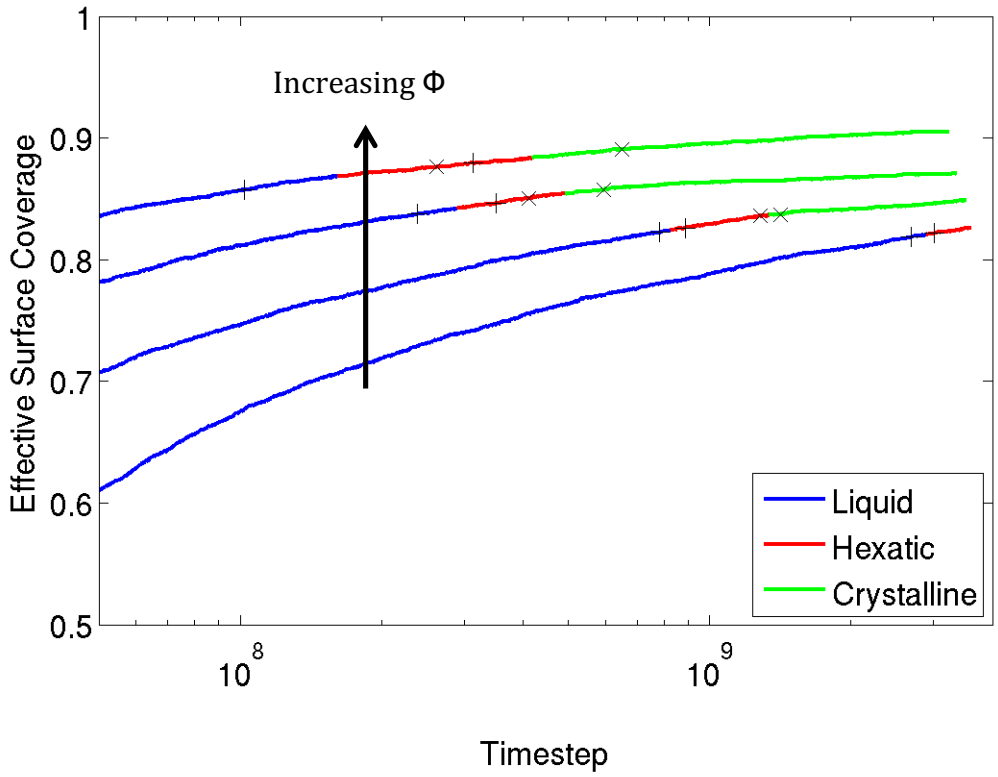

Figure 4.2 – Averaged adsorption curve for Brownian Dynamic simulations with bulk concentrations of 0.05, 0.07, 0.09, and 0.11 showing the liquid-hexatic and hexatic-crystalline transition points. For each bulk concetration, the liquid phase is shown in blue, the hexatic phase is shown in red, and the crystalline phase is shown in green. Uncertainty ranges are shown as + markers for the liquid-hexatic phase and x markers for the hexatic crystalline phase.

potential. The transition point was independent of bulk concentration[14]–[17].

The 3D Brownian dynamics simulations presented here show that at constant particle-particle and particle-wall potentials, the order-disorder transition points are dependent on bulk concentration. To the author's knowledge, this is the first time precise liquid-hexatic and hexatic-crystalline transition points have

been determined in 3D Brownian dynamics simulations of adsorption of repulsively charged particles onto an attractive surface. Larger simulation size and use of the bond orientational correlation function demonstrates the importance of the bulk on in the in-plane ordering process of the surface.

The critical effective surface coverage and timestep at the liquid-hexatic and hexatic-crystalline transition points for each bulk concentration are plotted in figure 4.3 and 4.4, respectively. For both transition points, the critical effective surface coverage increases with increasing bulk concentration, while the critical timestep decreases with increasing bulk concentration. Both trends assist in offering an explanation of the importance of the bulk on the kinetically-limited ordering process. At higher concentrations, more particles would be present in the region directly above the adsorbed surface, leading to two proposed potential driving factors.

The first proposed driving factor is the rate of particle adsorption. A competition between adsorption rate and in-plane diffustion occurs. At higher concentrations the additional particles near the surface cause a faster rate of adsorption as clearly presented in the adsorption curves. This faster rate leads to a decreased critical timestep, but could also potentially prevent movement of particles on the surface into more energetically favorable positions due to additional particles adsorbing onto the surface. At high concentrations, particle adsorption interrupts the in- plane diffusion of particles until a critical point is

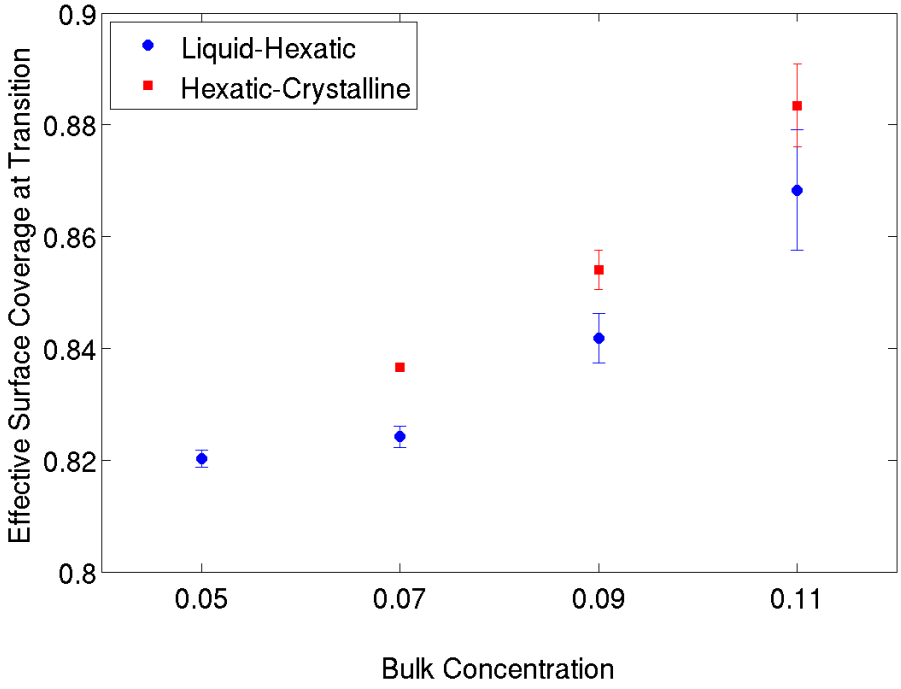

Figure 4.3 – Critical effective surface coverage at liquid-hexatic and hexatic-crystalline transition points for Brownian Dynamic simulations with bulk concentrations of 0.05, 0.07, 0.09, and 0.11

reached forcing the particles into an ordered state. Since all of the transition points occur at surface coverages significantly higher than the random sequential adsorption jamming limit and above the proposed order-disorder transition, it can be assumed that some diffusion of particles on the surface is occurring, but the diffusion is not occurring fast enough to form an ordered surface before additional particles are absorbed. The adsorbed particles in simulations with lower bulk concentrations have more time to diffuse on the surface before additional

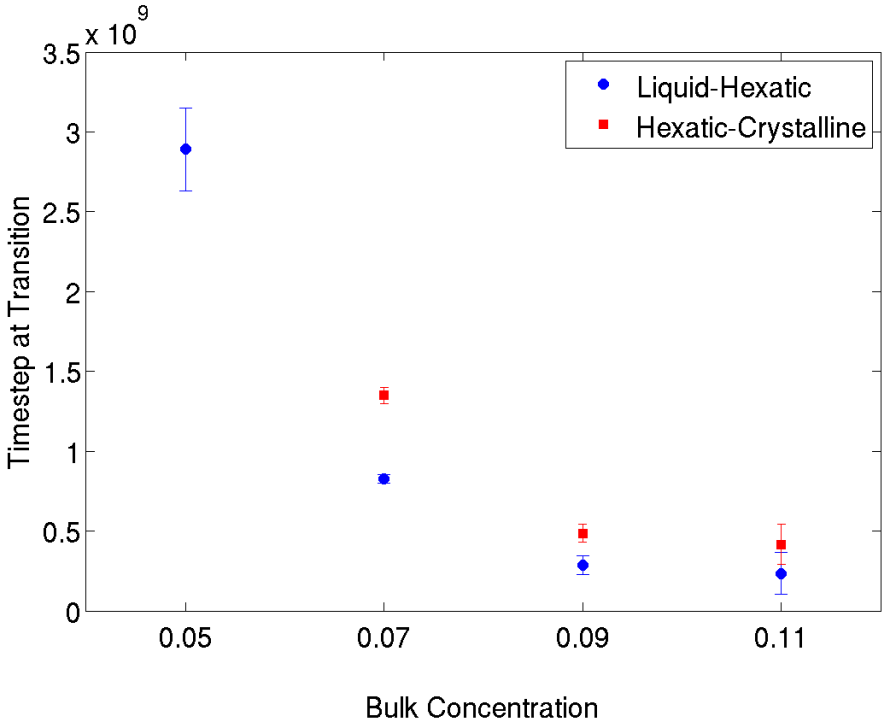

Figure 4.4 – Critical timestep at liquid-hexatic and hexatic-crystalline transition points for Brownian Dynamic simulations with bulk concentrations of 0.05, 0.07, 0.09, and 0.11

particles adsorb leading to a lower effective surface coverage at the liquid-hexatic and hexatic-crystalline transition points.

The second proposed driving factor is the interaction of the particles in the bulk close to the surface with the particles adsorbed on the surface. At higher concentrations, the repulsive interaction between the layer of particles immediately above surface and those on the surface prevent in-plane diffusion of some of the particles on the surface leading to further adsorption before order

occurs. This is an extension of the one-directional average force proposed by Miyahara et al., which states that there is a critical force required for the last adsorbing particle to overcome before the order-disorder transition occurs [15]–[17]. The one-directional average force is calculated as the average force required by a single adsorbing particle to push particles on the surface. It does not, however, take into account other particles in the bulk and their help or hindrance to pushing particles on the surface. At lower bulk concentrations, fewer particles would be present immediately above the surface, so less effect would be felt. At extremely low bulk concentrations, the one-directional average force might be sufficient if a negligible number of particles are present above the surface. A 3D force balance would be required to test this proposal.

Miyahara et al. completed a probability study demonstrating that the process during the last adsorption of a particle before ordering is characteristic of stochastic phenomenon. With respect to the critical timestep, the adsorption process was reported to have an exponential-type distribution of the probability. It was determined that it would be difficult to establish a critical timestep for the disorder-order transition and that the distribution of the critical timestep increases with decreasing bulk concentration [16], [17]. However, the uncertainty shown in Figure 4.4, suggests that for bulk concentrations above 0.05, the critical timestep can be determined, but the stochastic phenomenon prevents determination of a critical timestep for low bulk concentrations.

Interestingly, the uncertainty in the critical effective coverage at the transition points increases with increasing bulk concentration as shown in Figure 4.3. This suggests that for high concentrations, stochastic adsorption occurs much faster than in-plane diffusion. After a critical time, ordering occurs independent of effective surface coverage. This trend supports the first proposed driving factor of the bulk.

The stochastic nature of the adsorption process and the role of the bulk greatly influence the liquid-hexatic and hexatic-crystalline phase transition points. For low bulk concentrations, the critical effective surface coverage has low uncertainty, while the critical timestep does not. For high bulk concentration, the critical timestep has low uncertainty, while the critical effective surface coverage does not. These results further exemplify the complex importance of the bulk on the ordering process.

Using the critical effective surface coverage, a phase diagram can be constructed as shown in Table 4.2. The larger uncertainty in determining the transition points for bulk concentration 0.11 is evident in the phase diagram. To further verify the proposed phase diagram, particle ordering was further analyzed at 0.82, 0.83, 0.84, 0.85, 0.86, and 0.87 effective surface coverages. For each bulk concentration, all of the analysis presented was performed using one of the three Brownian dynamics simulations performed with different initial random particle placement. The snapshot analyzed was chosen randomly from

Table 4.2 – Phase diagram for Brownian Dynamic simulations with bulk concentrations of 0.05, 0.07, 0.09, and 0.11

Effective Surface Coverage, θ	Number of Adsorbed Particles, n	Φ = 0.11	Φ = 0.09	Φ = 0.07	Φ = 0.05
0.810	2017	L	L	L	L
0.815	2029	L	L	L	L
0.820	2042	L	L	L	L H
0.825	2054	L	L	L H	H
0.830	2067	L	L	H	H
0.835	2079	L	L	C	
0.840	2091	L	L H	C	
0.845	2104	L	L H	C	
0.850	2116	L	L H	C	
0.855	2129	L	H C		
0.860	2141	L H	C		
0.865	2154	L H	C		
0.870	2166	L H C	C		

all of the timesteps with the appropriate effective surface coverage. Additional analysis to ensure the data presented is representative of the system was performed, but is not presented to avoid unnecessary repetition.

Figure 4.5 and Figure 4.6 show the bond orientational correlation function for each of the bulk concentrations at increasing effective surface coverages. The averaged adsorption curves are given for each effective surface coverage for reference. Figures 4.7 – 4.12 show the corresponding Voronoi diagram and 2D structure factor for each of the bond orientational correlation functions presented in Figures 4.5 and 4.6.

At an effective surface coverage of 0.82, the surface order for all of the simulations are in the liquid phase. At larger effective surface coverage, the dependence of the bulk on ordering becomes apparent. Effective surface coverages of 0.84 and 0.85 exemplify this importance. At both effective surface coverages the simulation with bulk concentration of 0.11 is in the liquid phase, the simulation with bulk concentration of 0.09 is in the hexatic phase, and the simulation with bulk concentration of 0.07 is in the crystalline phase during the adsorption process.

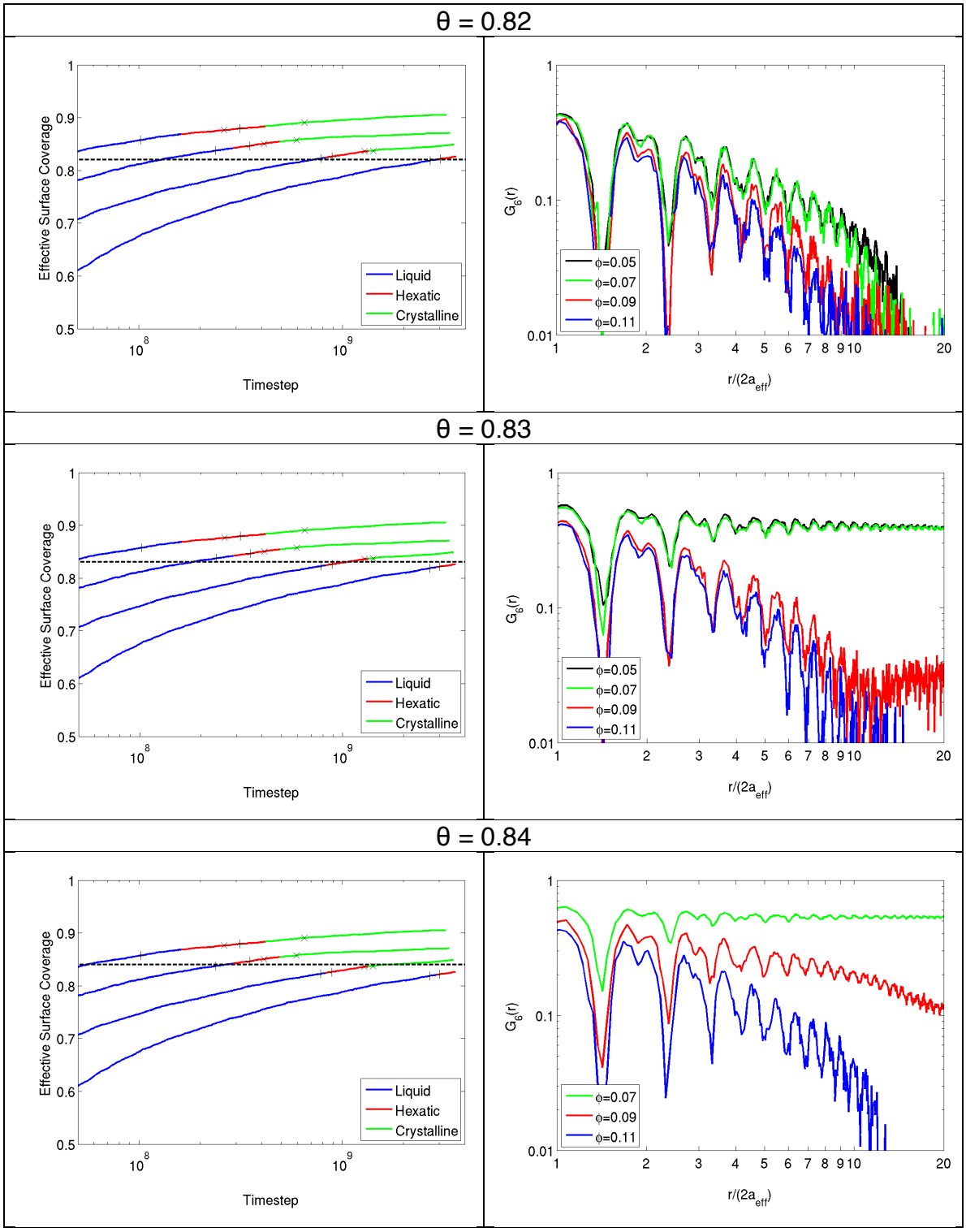

Figure 4.5 – Bond orientational correlation function for Brownian Dynamic simulations with bulk concentrations of 0.05, 0.07, 0.09, and 0.11 at effective surface coverages of 0.82, 0.83, and 0.84

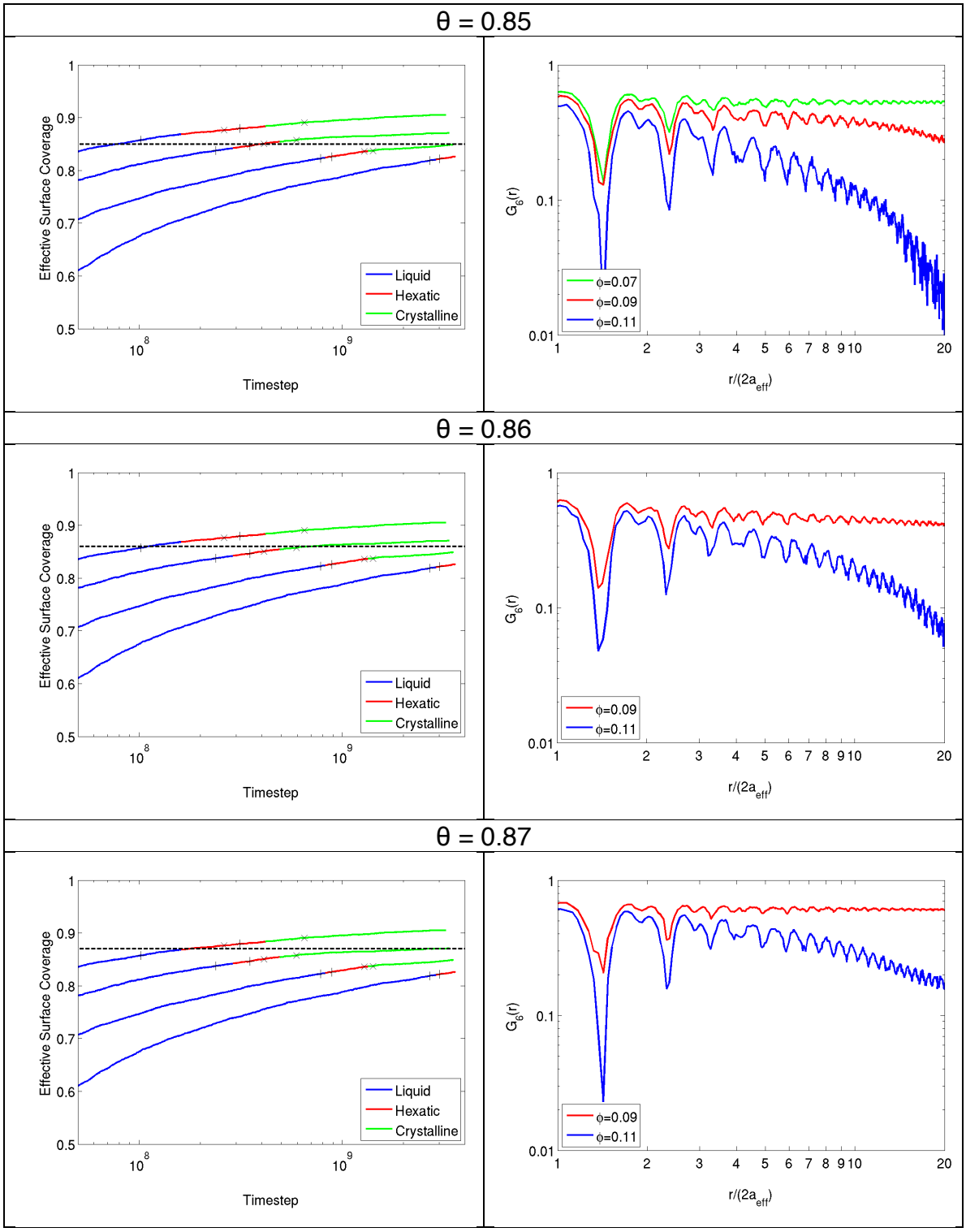

Figure 4.6 – Bond orientational correlation function for Brownian Dynamic simulations with bulk concentrations of 0.05, 0.07, 0.09, and 0.11 at effective surface coverages of 0.85, 0.86, and 0.87

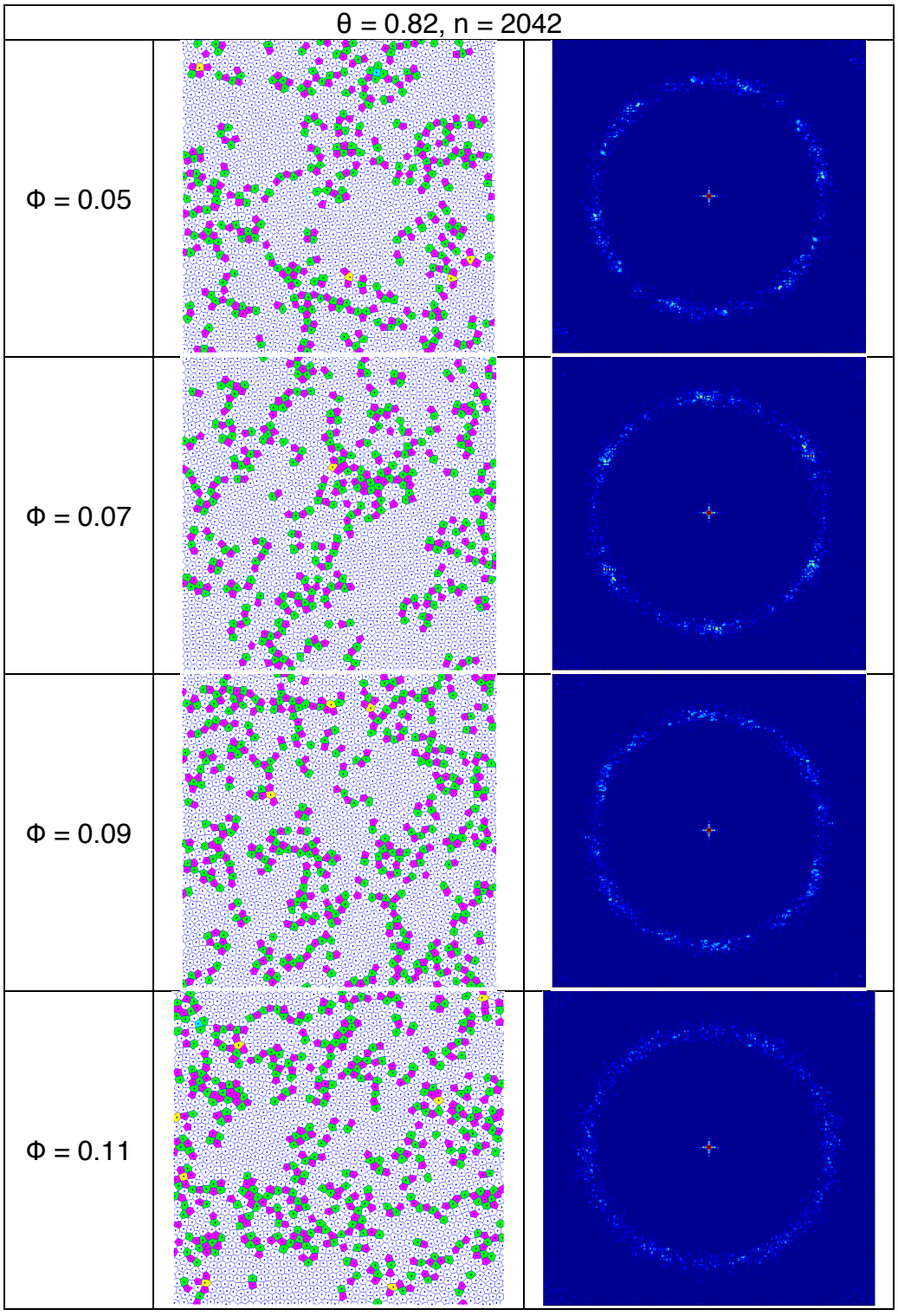

Figure 4.7 – Voronoi diagram and 2D structure factor for Brownian Dynamic simulations with bulk concentrations of 0.05, 0.07, 0.09, and 0.11 at effective surface coverage of 0.82 corresponding to the bond orientational correlation function in Figure 4.5

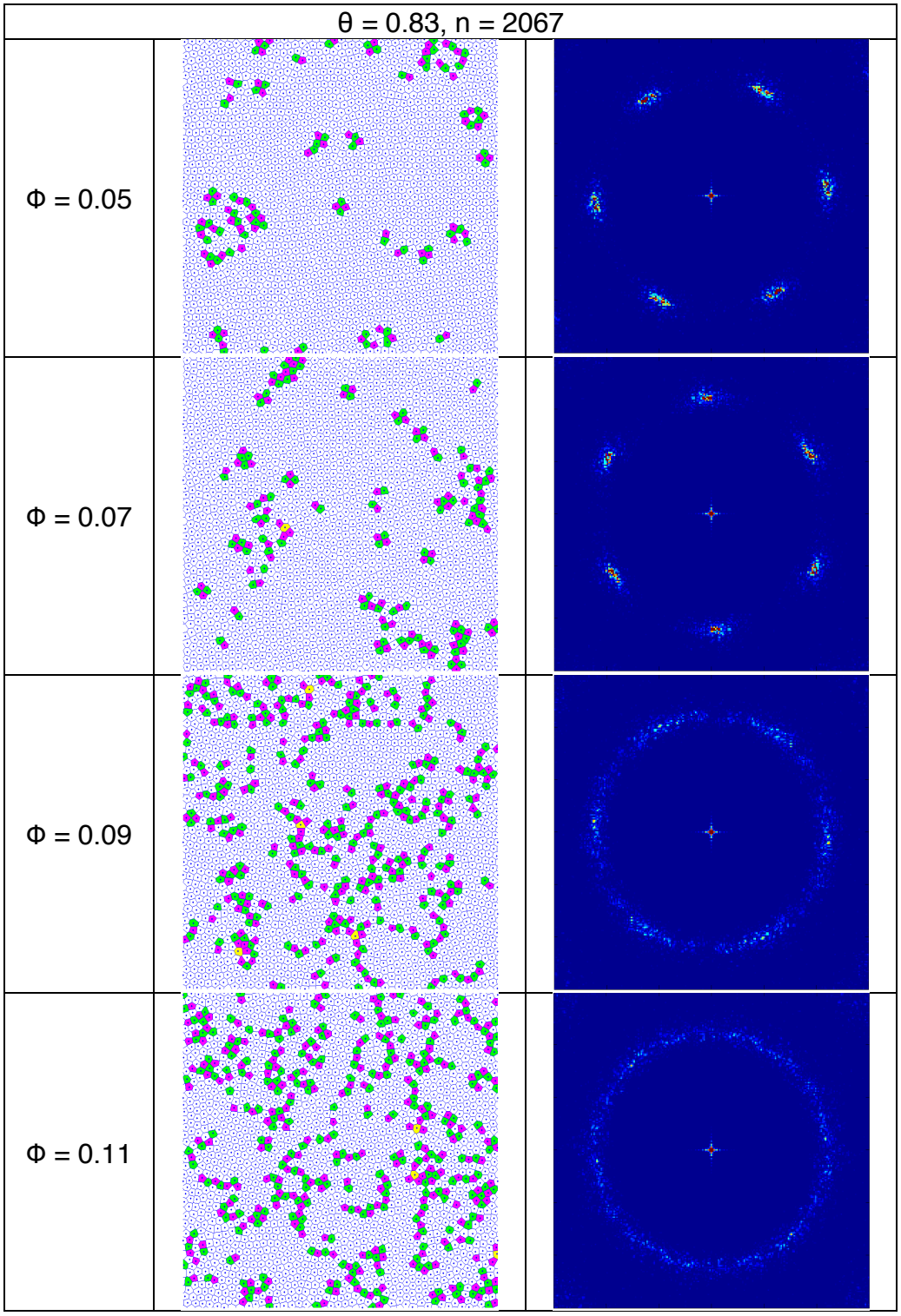

Figure 4.8 – Voronoi diagram and structure factor for Brownian Dynamic simulations with bulk concentrations of 0.05, 0.07, 0.09, and 0.11 at effective surface coverage of 0.83 corresponding to the bond orientational correlation function in Figure 4.5

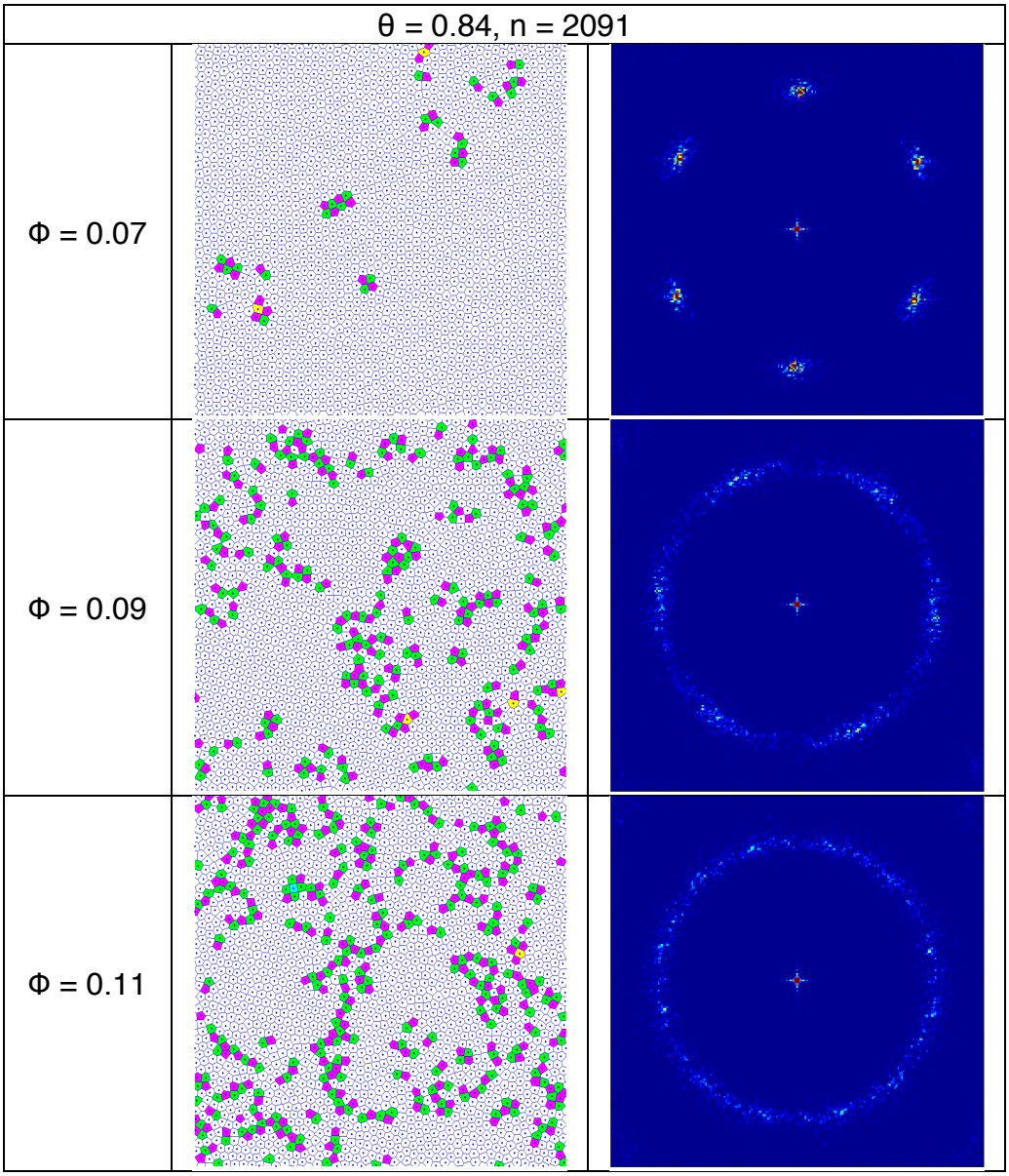

Figure 4.9 – Voronoi diagram and 2D structure factor for Brownian Dynamic simulations with bulk concentrations of 0.05, 0.07, 0.09, and 0.11 at effective surface coverage of 0.84 corresponding to the bond orientational correlation function in Figure 4.5

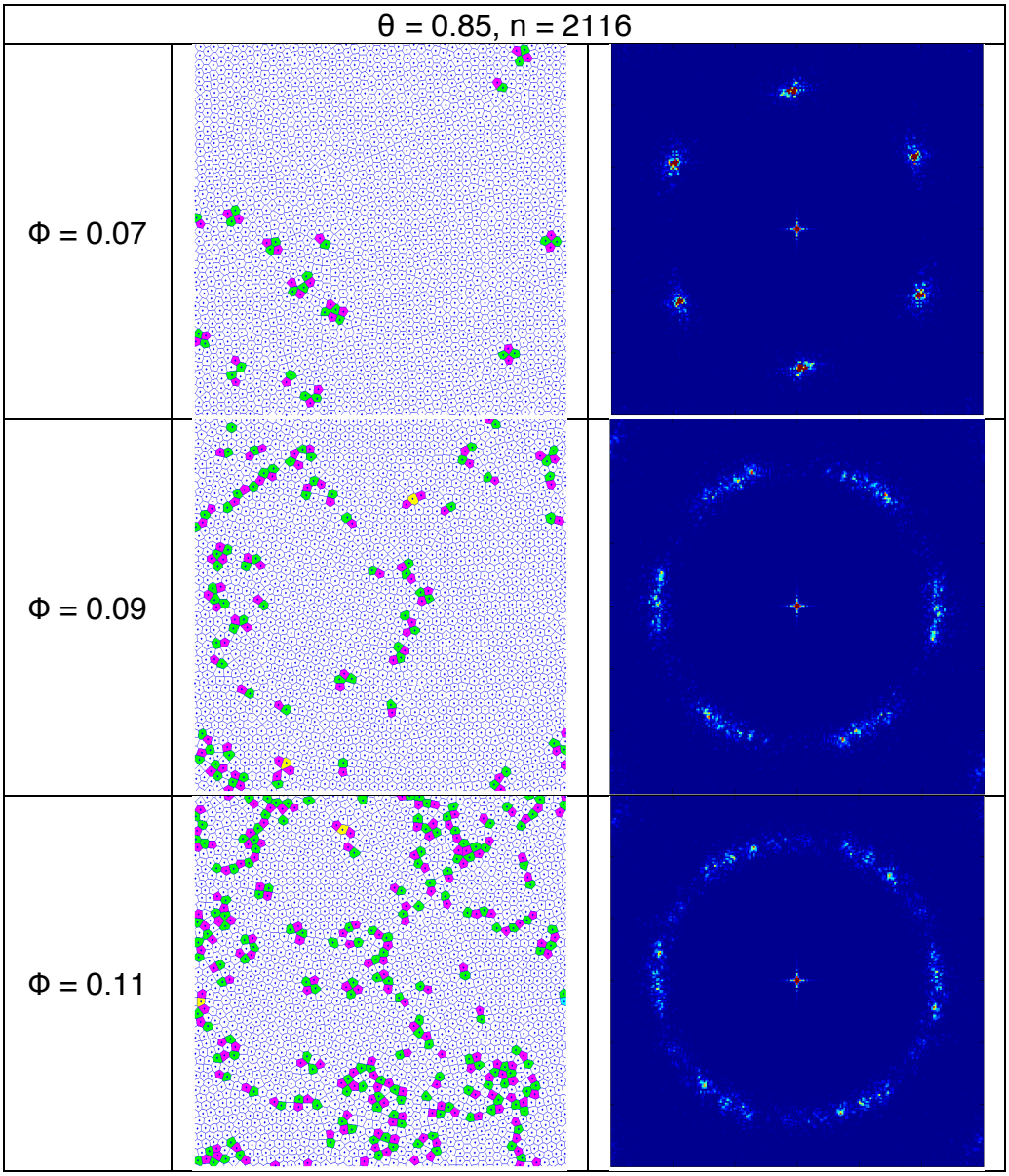

Figure 4.10 – Voronoi diagram and 2D structure factor for Brownian Dynamic simulations with bulk concentrations of 0.05, 0.07, 0.09, and 0.11 at effective surface coverage of 0.85 corresponding to the bond orientational correlation function in Figure 4.6

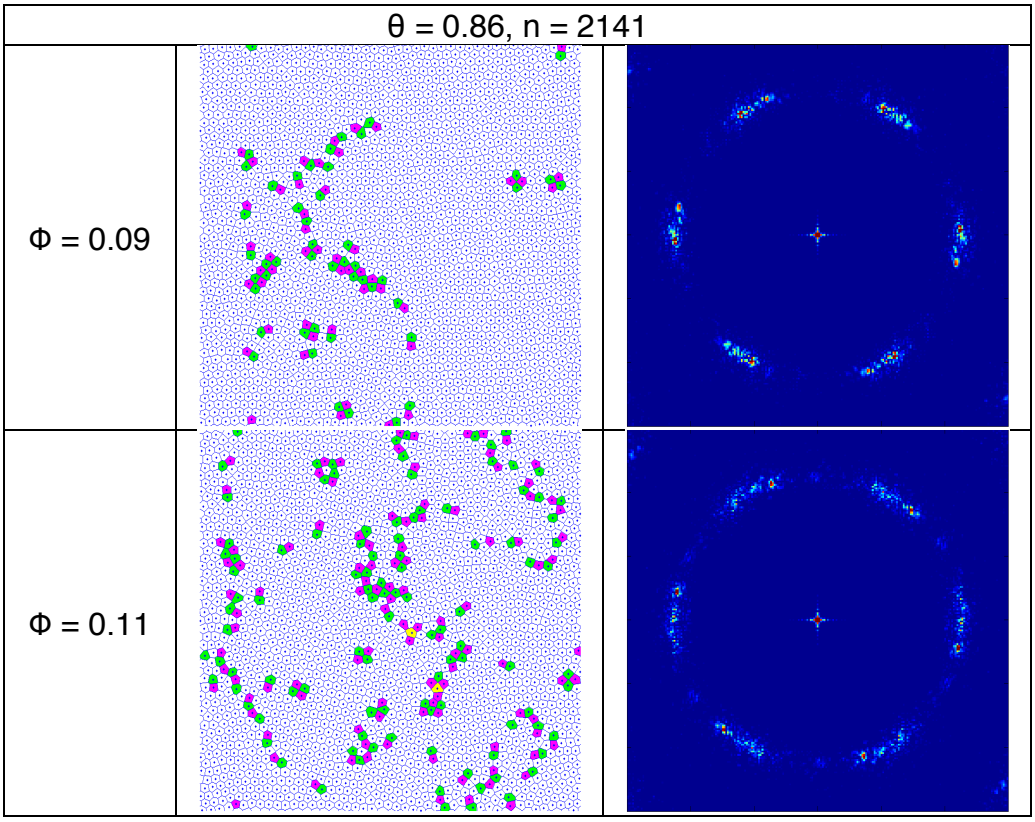

Figure 4.11 – Voronoi diagram and 2D structure factor for Brownian Dynamic simulations with bulk concentrations of 0.05, 0.07, 0.09, and 0.11 at effective surface coverage of 0.86 corresponding to the bond orientational correlation function in Figure 4.6

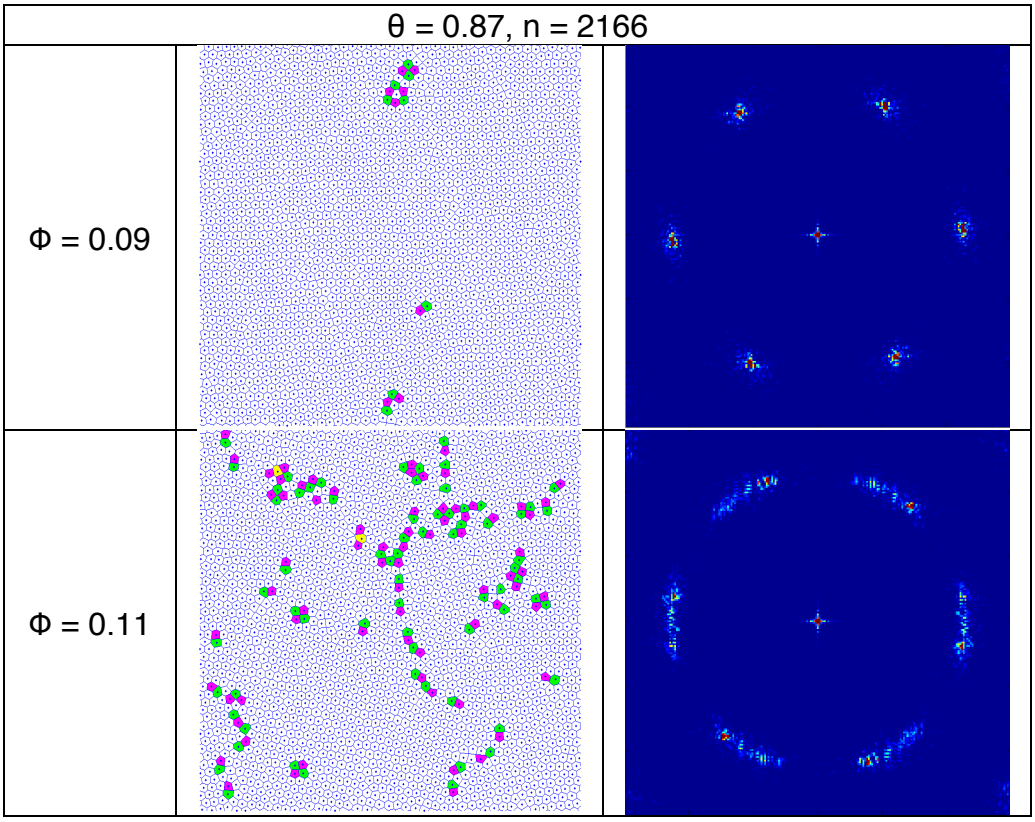

Figure 4.12 – Voronoi diagram and 2D structure factor for Brownian Dynamic simulations with bulk concentrations of 0.05, 0.07, 0.09, and 0.11 at effective surface coverage of 0.87 corresponding to the bond orientational correlation function in Figure 4.7

4.2. Fast Lubrication dynamics

Previous adsorption studies have ignored particle-particle hydrodynamic interactions in the bulk stating that particles are kept far enough apart due to the repulsive electrostatic double-layer or low bulk concentration [14]–[17]. The role of particle-particle hydrodynamic interactions could however effect in-plane movement of the adsorbed particle, especially as increased surface coverage is achieved. The aim of this study is to determine if hydrodynamic interactions between particles effect the ordering process during adsorption. To the author's knowledge, this is the first time particle-particle hydrodynamics interactions have been included in 3D simulations of significant size to analyze the adsorption and ordering of repulsively charged particles onto an attractive surface.

4.2.1. Bulk Movement

Given previous literature, it was expected that the addition of particle-particle hydrodynamic interactions would have no significant effect on bulk movement. For each simulation, the diffusion coefficient was calculated using the Einstein relation from the mean-squared displacement of particles during the equilibration step with all periodic boundary conditions [42]. The calculated diffusion coefficients for the Brownian dynamics and Fast Lubrication dynamics simulations are given in Table 4.3. Unexpectedly, the addition of particle-particle hydrodynamic interactions did alter the bulk movement of particles. The Fast

Lubrication dynamics simulations have bulk movement notably slower than Brownian Dynamic simulation with the same bulk concentration. As would be expected, the effect of particle-particle hydrodynamic interactions on the diffusion coefficient increased with increasing bulk concentration.

Given the diffusion coefficients in Table 4.3, it is expected that adsorption curves for the Fast Lubrication dynamics simulations will slightly lag the adsorption curves of the Brownian dynamics simulations at the same bulk concentration due to a lag in the early diffusion limited adsorption regime. The

Table 4.3 – Bulk diffusion coefficient for the Brownian dynamics simulations and the Fast Lubrication dynamics simuations calculated using all periodic boundary conditions

	Φ	Diffusion Coefficient, D (nm^2/timestep)
BD 1	0.05	0.001344
BD 2	0.05	0.001307
BD 3	0.05	0.001338
BD 1	0.07	0.001130
BD 2	0.07	0.001140
BD 3	0.07	0.001118
FLD 1	0.07	0.000822
FLD 2	0.07	0.000826
BD 1	0.09	0.000900
BD 2	0.09	0.000909
BD 3	0.09	0.000906
FLD 1	0.09	0.000606
FLD 2	0.09	0.000597
BD 1	0.11	0.000670
BD 2	0.11	0.000677
BD 3	0.11	0.000668
FLD 1	0.11	0.000407
FLD 2	0.11	0.000413

reduced diffusion means particles adsorb at a slower rate, but after the initial diffusion limited adsorption regime, the number of particles in the layer directly above the adsorbed layer is relatively the same for a given bulk concentration regardless if hydrodynamic interactions are included or not. In the kinetically limited adsorption regime, particle should adsorb at the same rate observed in Brownian Dynamics simulations.

If the 2 proposed roles of the bulk in the ordering process suggested in section 4.1.2 are correct, the decreased diffusion coefficient should increase the uncertainty in the critical effective surface coverage at the liquid-hexatic and hexatic-crystalline phase transition points due to reduced in-plane diffusion with an unchanged adsorption rate when compared to the transition points observed in the Brownian dynamics simulations at the same bulk concentration. Since the particles in the layer directly above the adsorbed layer is relatively the same for a given bulk concentration regardless if hydrodynamic interactions are included or not at the transition points, only the first proposed driving factor of the bulk would be effected by the addition of particle-particle hydrodynamic interactions. Any effect of particle-particle hydrodynamic interactions on the ordering process should be a result of its effect on in-plane motion, not bulk movement.

4.2.2. Adsorption

One of the adsorption curves for each of the Fast Lubrication dynamics simulations as well as the Brownian dynamics simulations for bulk concentrations

0.07 and 0.09 are shown in Figure 4.13. The two Fast Lubrication dynamics adsorption curves shown are indicative of the adsorption curves for the other Fast Lubrication dynamics simulations, which have not been shown. As expected, the adsorption process for the Fast Lubrication dynamics simulations follows the adsorption process observed in the Brownian dynamics simulation.

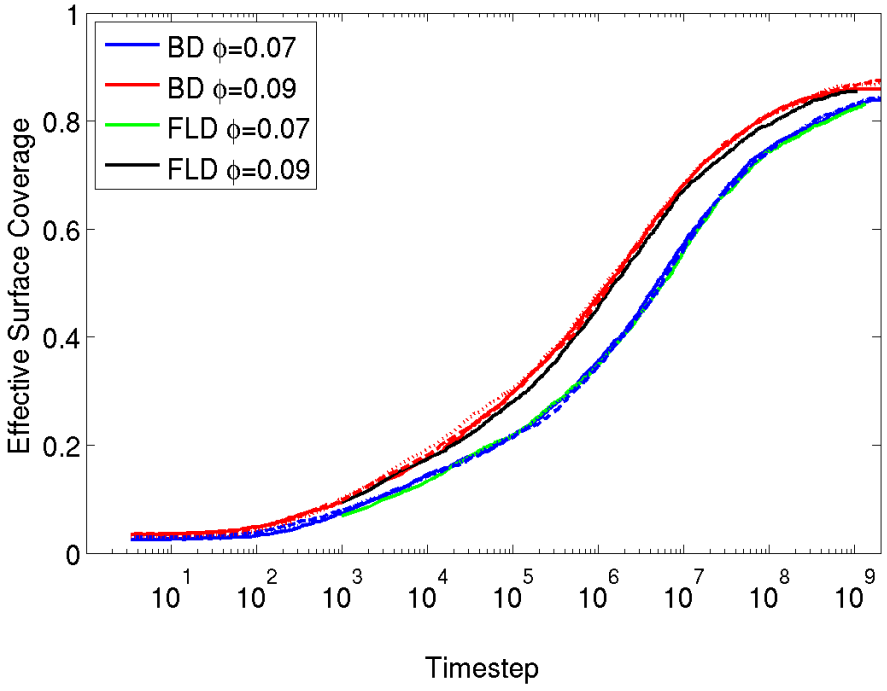

Figure 4.13 – Adsorption curves for Brownian Dynamic and Fast Lubrication dynamics simulations with bulk concentrations of 0.07 and 0.09. For each bulk concetration, the 3 Brownian dynamics simulations performed with different intial random particle placement as dotted, dashed, and solid lines in the same color.

Without detailed analysis of the early diffusion limited adsorption regime, it is impossible to determine if the slight lag in adsorption is a result of the lower diffusion coefficient or simply due to the stochastic nature of these simulations.

Table 4.4 – Transition points for Brownian Dynamic and Fast Lubrication dynamics simulations with bulk concentrations of 0.07 and 0.09.

	Φ	LIQUID-HEXATIC		HEXATIC-CRYSTALLINE	
		n	Timestep	n	Timestep
BD 1	0.07	2043	7.9500E+08	2079	1.4000E+09
BD 2	0.07	2059	8.8000E+08	2085	1.2500E+09
BD 3	0.07	2054	8.0000E+08	2085	1.4000E+09
FLD 1	0.07	2066	1.2832E+09	2080	1.5848E+09
FLD 2	0.07	2064	1.2498E+09	2079	1.7665E+09
BD 1	0.09	2083	2.3000E+08	2109	4.1000E+08
BD 2	0.09	2118	4.0000E+08	2135	6.0000E+08
BD 3	0.09	2087	2.3000E+08	2135	4.5000E+08
FLD 1	0.09	2070	2.8220E+08	2109	5.3980E+08
FLD 2	0.09	2091	4.3340E+08	2163	1.5832E+09
BD 1	0.11	2134	1.0500E+08	2213	5.0000E+08
BD 2	0.11	2216	5.0000E+08	2223	5.8000E+08
BD 3	0.11	2136	1.0000E+08	2163	1.7000E+08
FLD 1	0.11	2139	1.8650E+08	2166	3.1650E+08
FLD 2	0.11	2168	4.4175E+08	2205	7.7820E+08

4.2.1. Ordering

The bond orientational correlation function as well as the 2D structure factor was once again used to determine the liquid-hexatic and hexatic-crystalline transition point during the adsorption process. The number of particles adsorbed, n, and timestep at each transition point is given in Table 4.4. Data for the

Brownian dynamics simulations is repeated for convenience. The transition points for the Fast Lubrication dynamics simulations were determined carefully and demonstrate the need for multiple analysis methods in determining surface structure. Distinct grains formed during the adsorption process in some of the simulations making the bond orientational correlation function insufficient to determine the transition points on its own. Voronoi diagrams with examples of the grains formed are shown in Figure 4.14. Additional analysis is necessary to determine the role of these grains in the ordering process. Additional simulations would be required to determine if the grain formation is a result of particle-particle hydrodynamic interactions.

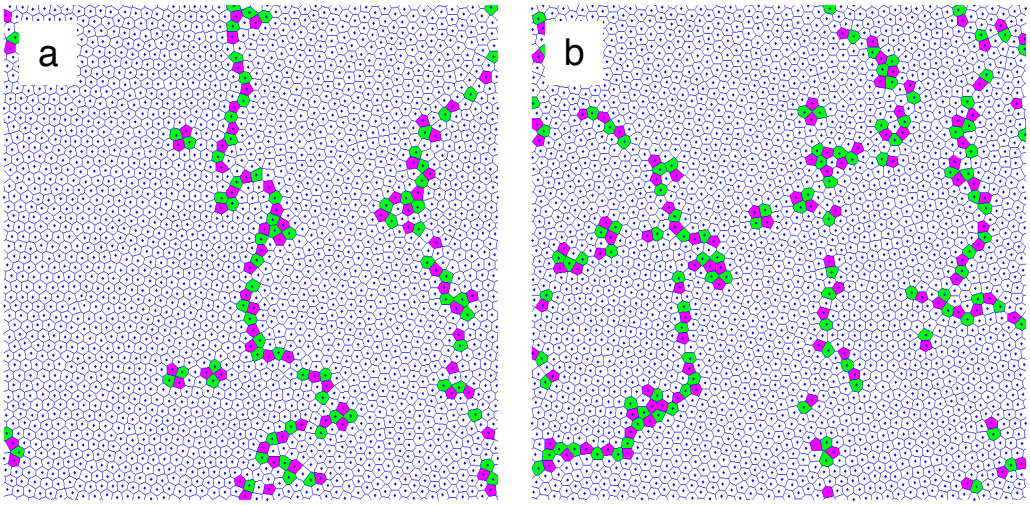

Figure 4.14 – Voronoi diagram showing grain formation during the adsoption process in Fast Lubrication dynamics simulations for a) bulk concentration of 0.09 with effective surface coverage of 0.86 and b) bulk concentration of 0.11 with effective surface coverage of 0.87

The critical effective surface coverage and timestep at the liquid-hexatic and hexatic-crystalline transition points for each bulk concentration are compared to those from the Brownian dynamics simulations in figure 4.15 and 4.16, respectively. The trends observed in the Brownian dynamics simulations are also present in the Fast Lubrication dynamics simulations. The critical effective surface coverage increases with increasing bulk concentration, while the critical timestep decreases with increasing bulk concentration. While additional simulations would be required to determine the uncertainty in the critical effective

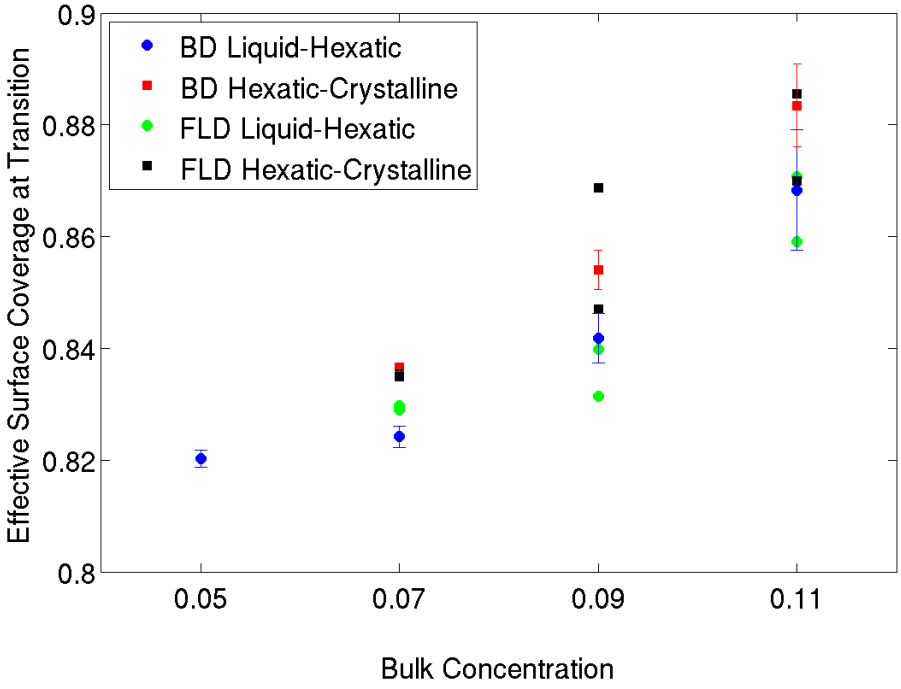

Figure 4.15 – Critical effective surface coverage at liquid-hexatic and hexatic-crystalline transition points comparing the Brownian Dynamic simulations with bulk concentrations of 0.05, 0.07, 0.09, and 0.11 with the Fast Lubrication dynamics simulations with bulk concentrations of 0.07 and 0.09

surface coverage at the transition points for the Fast Lubrication dynamics simulations, the data shown in Figure 4.15 supports the initial hypothesis of increasing uncertainty when compared to that of the Brownian dynamics simulations.

The uncertainty of the critical timestep for the Fast Lubrication dynamics simulations also appears to increase when compared to that of the Brownian dynamics simulations. In addition, the Fast Lubrication dynamics simulations appear to require longer timescales to reach the liquid-hexatic and hexatic-

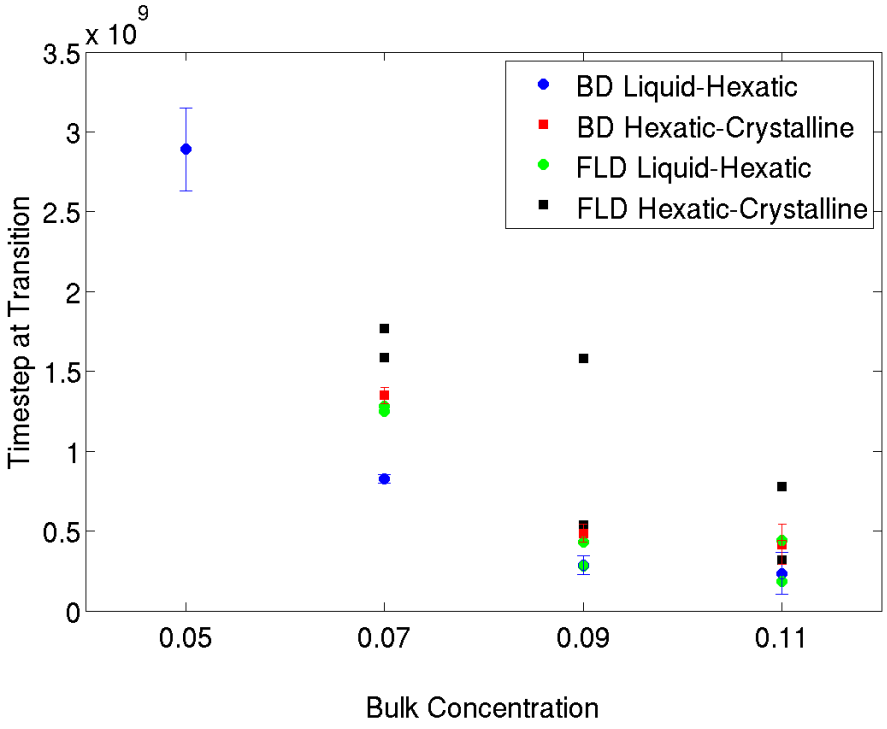

Figure 4.16 – Critical timestep at liquid-hexatic and hexatic-crystalline transition points comparing the Brownian Dynamic simulations with bulk concentrations of 0.05, 0.07, 0.09, and 0.11 with the Fast Lubrication dynamics simulations with bulk concentrations of 0.07 and 0.09

crystalline transition points. These initial results suggest that the particle-particle hydrodynamic interactions greatly alter the in-plane diffusion and movement of particles leading to longer timescales required for ordering and increased uncertainty in the critical effective surface coverage at the transition points.

Figure 4.17-4.19 compares examples of the Voronoi diagram and 2D structure factor from the Fast Lubrication dynamics simulations and Brownian dynamics simulations for each of the bulk concentrations at an effective surface coverage of 0.84. At an effective surface coverage of 0.84, it is evident that the Fast Lubrication dynamics simulations follow the same trends seen in the Brownian dynamics simulations. For both Brownian dynamics and Fast Lubrication dynamics simulations, the simulations with bulk concentration of 0.11 is in the liquid phase, the simulation with bulk concentration of 0.09 is in the hexatic phase, and the simulation with bulk concentration of 0.07 is in the crystalline phase during the adsorption process.

The importance of the bulk on the adsorption and ordering process is clear in both Brownian dynamics and Fast Lubrication dynamics simulations. Fast Lubrication dynamics simulations add to the complexity of the bulk's interaction with the adsorbed particles on the surface and therefore also with the ordering process. In both simulations, liquid-hexatic and hexatic-crystalline transition points are dependent on bulk concentration. Distinct grains formed during the adsorption and ordering process in the Fast Lubrication dynamics simulations

suggests that particle-particle hydrodynamics interactions might influence the mechanism responsible for ordering. Additional analysis of the defect structure could help identify the role of particle-particle hydrodynamic interactions in the ordering process. Additional simulations including hydrodynamics with different solvents would need to be completed before any definitive trends concerning the role of particle-particle hydrodynamics on the in-plane ordering process could be stated.

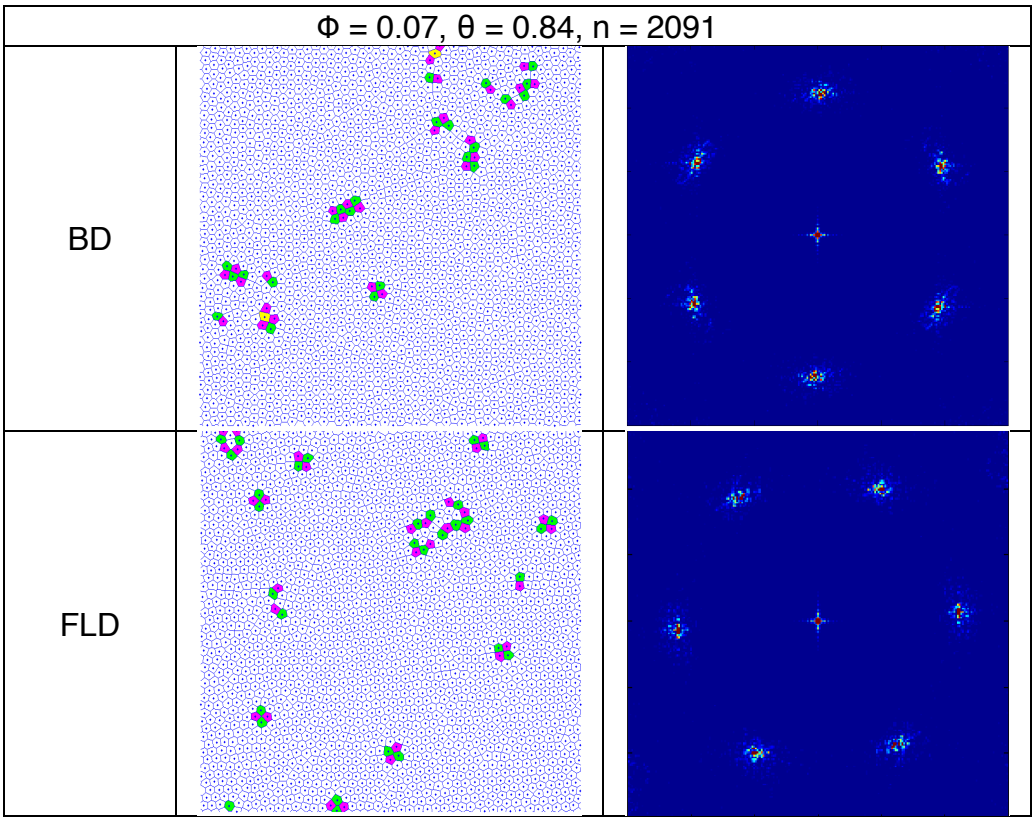

Figure 4.17 – Voronoi diagram and structure factor comparing the Brownian dynamics simulation with the Fast Lubrication dynamics simuation for a bulk concentration of 0.07 at effective surface coverage of 0.84

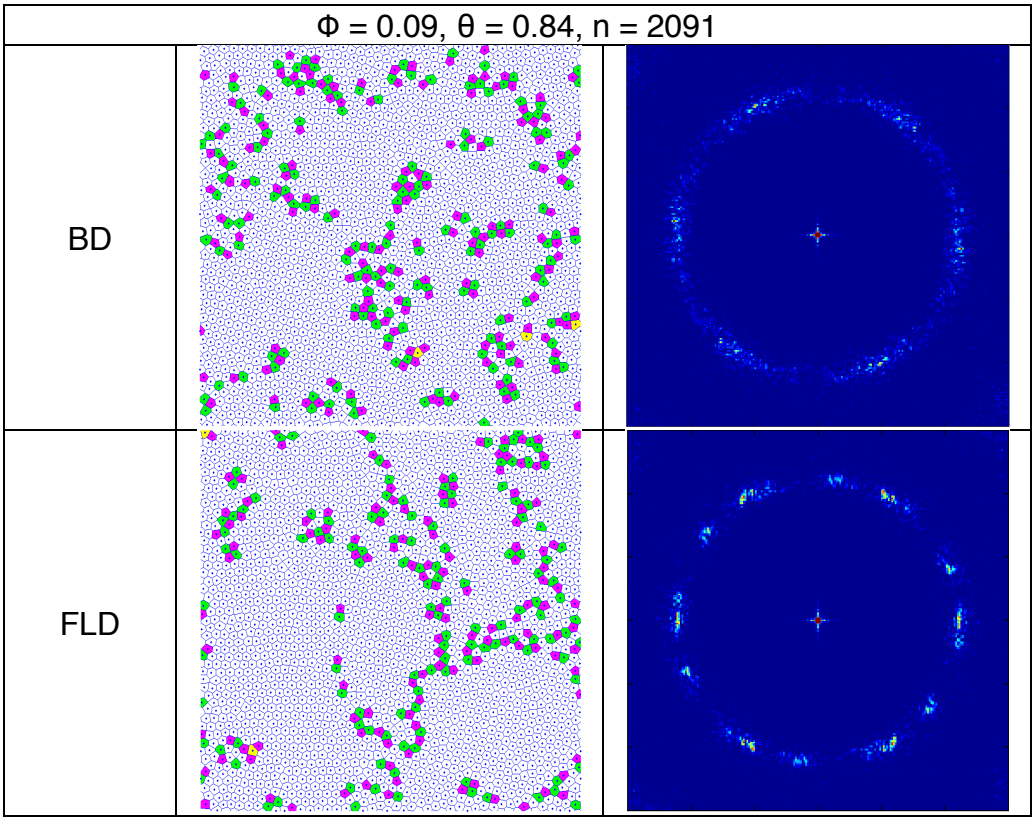

Figure 4.18 – Voronoi diagram and structure factor comparing the Brownian dynamics simulation with the Fast Lubrication dynamics simuation for a bulk concentration of 0.09 at effective surface coverage of 0.84

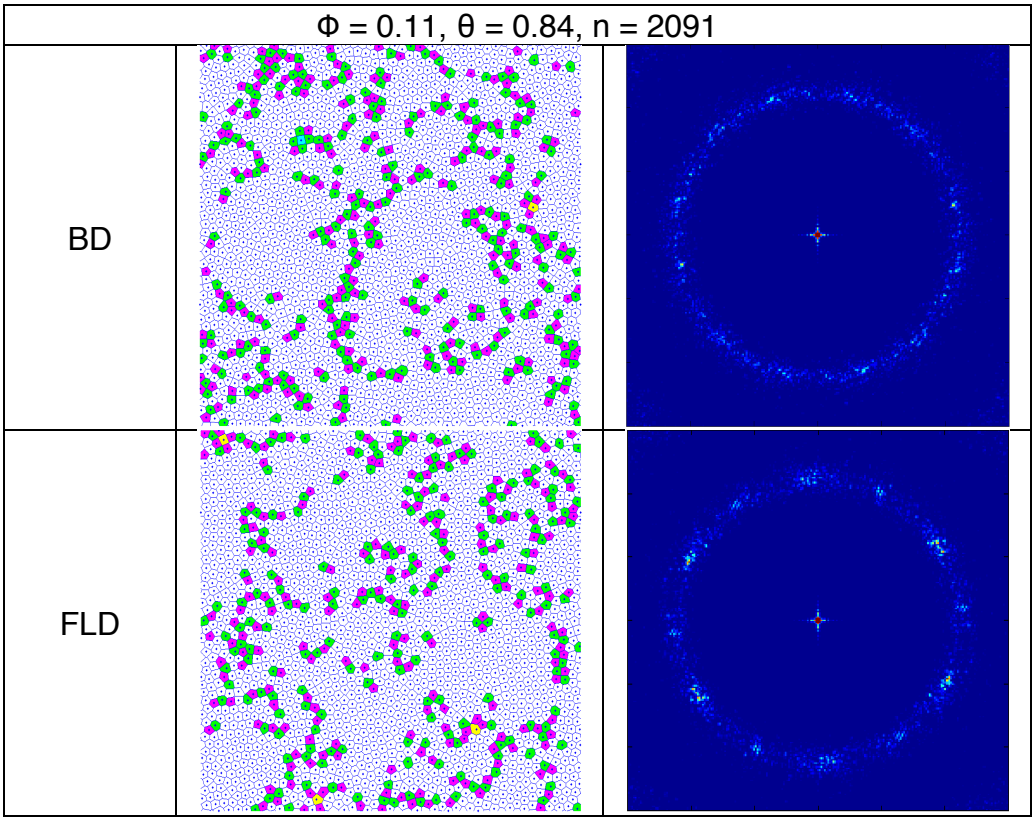

Figure 4.19 – Voronoi diagram and structure factor comparing the Brownian dynamics simulation with the Fast Lubrication dynamics simuation for a bulk concentration of 0.11 at effective surface coverage of 0.84

Chapter 5

Conclusions & Future Work

5.1. Conclusions

3D Brownian dynamics and Fast Lubrication dynamics simulations of electrostatically stabilized nanoparticles onto an attractive surface with varying bulk concentrations of the nanoparticles in solution were analyzed and the transition points between between liquid, hexatic, and crystalline nanoparticle arrays were identified. Previous simulations have shown that tuning particle and surface potentials, screening lengths, and particle concentrations can lead to ordering. The Brownian dynamics and Fast Lubrication dynamics simulations analyzed show that the order-disorder transition is also greatly impacted by the bulk. For all simulations, adsorption was irreversible and the particles diffused laterally on the surface. Liquid, hexatic, and crystalline phases were observed in

both the Brownian dynamics and Fast Lubrication dynamics simulations. Both simulations also demonstrated that the critical effective surface coverage required for the liquid-hexatic or hexatic-crystalline transition point increases with increasing bulk concentration, while the critical timestep decreases with increasing bulk concentration exposing the importance of bulk concentration in the ordering process. Fast Lubrication dynamics simulations demonstrate the complex role of not only the bulk concentration but also the bulk solvent on the ordering process. Initial results suggest that the addition of hydrodynamic interactions between particles might increase the stochastic nature of the adsorption and ordering process requiring several runs to determine the uncertainty associated with identifying the critical timestep and effective surface coverage for the liquid-hexatic and hexatic-crystalline transition point. Additional defect analysis may give insight to mechanisms responsible for ordering.

5.2. Future Work

Additional simulations and analysis would further elucidate the mechanism responsible for the timing and effective surface coverage required for the order-disorder transition to occur. The simulations presented varied bulk concentrations and could be expanded by varying the Debye length, temperature, or surface potential. As mentioned in the analysis, additional Fast Lubrication dynamics simulations using the described system as well as systems using different

solvents are required to understand the role of particle-particle hydrodynamic interactions on the ordering process.

In addition, simulations could be expanded to more accurately represent experimental systems. The described system could be expanded by adding friction to the surface or particle-surface hydrodynamic interactions. Bi-dispersed or multi-dispersed nanoparticles as well as non-spherical particles could be simulated. It should be noted that new techniques for determining the liquid-hexatic and hexatic-crystalline transition points would need to be developed for polydispersed or non-spherical particles. The exploration of other particle-particle potential curves, especially those that that contain local minimums could result in surface patterns other than closed packed, which is of particular interest to many industries. Current methods of adsorption onto patterned surfaces could be improved from simulations leading to pattern optimization and better control of adsorption.

Additional analysis techniques have the potential to determine the role of the bulk on the driving factor leading to the liquid-hexatic and hexatic-crystalline transition. Extending the “one-directional average force” proposed by Miyahara et al. to include a three dimensional force balance of each system at the liquid-hexatic and hexatic-crystalline phase transition could provide significant understanding of the ordering process.

References

[1] F. Rogers, *The World According to Mister Rogers: Important Things to Remember*. Hachette Books, 2003.

[2] J. Feder, "Random sequential adsorption," *Journal of Theoretical Biology*, vol. 87, no. 2, pp. 237–254, Nov. 1980.

[3] E. L. Hinrichsen, J. Feder, and T. Jøssang, "Geometry of random sequential adsorption," *Journal of statistical physics*, vol. 44, no. 5–6, pp. 793–827, 1986.

[4] M. R. Oberholzer, J. M. Stankovich, S. L. Carnie, D. Y. C. Chan, and A. M. Lenhoff, "2-D and 3-D Interactions in Random Sequential Adsorption of Charged Particles," *Journal of Colloid and Interface Science*, vol. 194, no. 1, pp. 138–153, Oct. 1997.

[5] I. Pagonabarraga and J. M. Rubi, "Adsorption of colloidal particles: influence of transport (hydrodynamic interactions)," *Colloids and Surfaces A: Physicochemical and Engineering Aspects*, vol. 127, no. 1, pp. 249–255, 1997.

[6] J. J. Gray, D. H. Klein, B. A. Korgel, and R. T. Bonnecaze, "Microstructure Formation and Kinetics in the Random Sequential Adsorption of Polydisperse Tethered Nanoparticles Modeled as Hard Disks," *Langmuir*, vol. 17, no. 8, pp. 2317–2328, Apr. 2001.

[7] Z. Adamczyk, B. Siwek, M. Zembala, and P. Weroński, "Influence of polydispersity on random sequential adsorption of spherical particles," *Journal of colloid and interface science*, vol. 185, no. 1, pp. 236–244, 1997.

[8] Z. Adamczyk, M. Nattich, and J. Barbasz, “Deposition of colloid particles at heterogeneous and patterned surfaces,” *Advances in Colloid and Interface Science*, vol. 147–148, pp. 2–17, Mar. 2009.

[9] G. Malescio and G. Pellicane, “Stripe phases from isotropic repulsive interactions,” *Nat Mater*, vol. 2, no. 2, pp. 97–100, Feb. 2003.

[10] P. J. Camp, “Structure and phase behavior of a two-dimensional system with core-softened and long-range repulsive interactions,” *Phys. Rev. E*, vol. 68, no. 6, p. 061506, Dec. 2003.

[11] G. Malescio and G. Pellicane, “Stripe patterns in two-dimensional systems with core-corona molecular architecture,” *Phys. Rev. E*, vol. 70, no. 2, p. 021202, Aug. 2004.

[12] M. A. Glaser, G. M. Grason, R. D. Kamien, A. Košmrlj, C. D. Santangelo, and P. Ziherl, “Soft spheres make more mesophases,” *EPL*, vol. 78, no. 4, p. 46004, 2007.

[13] M. R. Oberholzer, N. J. Wagner, and A. M. Lenhoff, “Grand canonical Brownian dynamics simulation of colloidal adsorption,” *The Journal of Chemical Physics*, vol. 107, no. 21, pp. 9157–9167, Dec. 1997.

[14] J. J. Gray and R. T. Bonnecaze, “Adsorption of colloidal particles by Brownian dynamics simulation: Kinetics and surface structures,” *The Journal of Chemical Physics*, vol. 114, no. 3, p. 1366, 2001.

[15] M. Miyahara, S. Watanabe, Y. Gotoh, and K. Higashitani, “Adsorption and order formation of colloidal nanoparticles on a substrate: A Brownian dynamics study,” *The Journal of Chemical Physics*, vol. 120, no. 3, p. 1524, 2004.

[16] S. Watanabe, M. Miyahara, and K. Higashitani, "Dynamics of order formation by colloidal adsorption onto a substrate studied with Brownian dynamics," *The Journal of Chemical Physics*, vol. 122, no. 10, p. 104704, 2005.

[17] M. Miyahara, S. Watanabe, and K. Higashitani, "Modeling adsorption and order formation by colloidal particles on a solid surface: A Brownian dynamics study," *Chemical Engineering Science*, vol. 61, no. 7, pp. 2142–2149, Apr. 2006.

[18] J. J. Gray and R. T. Bonnecaze, "Adsorption of Charge-Bidisperse Mixtures of Colloidal Particles," *Langmuir*, vol. 17, no. 25, pp. 7935–7947, Dec. 2001.

[19] D. D. Brewer, M. Tsapatsis, and S. Kumar, "Dynamics of surface structure evolution in colloidal adsorption: Charge patterning and polydispersity," *The Journal of Chemical Physics*, vol. 133, no. 3, p. 034709, 2010.

[20] S. Watanabe and M. T. Miyahara, "Order formation of colloidal nanoparticles adsorbed on a substrate with friction," *Advanced Powder Technology*, vol. 21, no. 1, pp. 57–63, Jan. 2010.

[21] P. J. Hoogerbrugge and J. M. V. A. Koelman, "Simulating Microscopic Hydrodynamic Phenomena with Dissipative Particle Dynamics," *EPL*, vol. 19, no. 3, p. 155, 1992.

[22] A. J. C. Ladd, "Numerical simulations of particulate suspensions via a discretized Boltzmann equation. Part 1. Theoretical foundation," *Journal of Fluid Mechanics*, vol. 271, pp. 285–309, Jul. 1994.

[23] D. L. Ermak and J. A. McCammon, “Brownian dynamics with hydrodynamic interactions,” *The Journal of Chemical Physics*, vol. 69, no. 4, pp. 1352–1360, Aug. 1978.

[24] J F Brady and and G. Bossis, “Stokesian Dynamics,” *Annual Review of Fluid Mechanics*, vol. 20, no. 1, pp. 111–157, 1988.

[25] A. Sierou and J. F. Brady, “Accelerated Stokesian Dynamics simulations,” *Journal of Fluid Mechanics*, vol. 448, pp. 115–146, Dec. 2001.

[26] A. Kumar and J. J. L. Higdon, “Origins of the anomalous stress behavior in charged colloidal suspensions under shear,” *Phys. Rev. E*, vol. 82, no. 5, p. 051401, Nov. 2010.

[27] A. Kumar, “Microscale dynamics in suspensions of non-spherical particles.” Thesis, University of Illinois Urbana-Champaign, 2010.

[28] S. Plimpton, “Fast Parallel Algorithms for Short-Range Molecular Dynamics,” *Journal of Computational Physics*, vol. 117, no. 1, pp. 1–19, Mar. 1995.

[29] W. B. Russel, D. A. Saville, and W. R. Schowalter, *Colloidal Dispersions*. Cambridge University Press, 1992.

[30] D. Frenkel and B. Smit, *Understanding Molecular Simulation: From Algorithms to Applications*. Academic Press, 2001.

[31] J. Israelachvili, *Intermolecular and Surface Forces*, Third Edition. Academic Press, 2011.

[32] J. E. Sader, “Accurate analytic formulae for the far field effective potential and surface charge density of a uniformly charged sphere,” *Journal of colloid and interface science*, vol. 188, no. 2, pp. 508–510, 1997.

[33] G. M. Bell, S. Levine, and L. N. McCartney, “Approximate methods of determining the double-layer free energy of interaction between two charged colloidal spheres,” *Journal of Colloid and Interface Science*, vol. 33, no. 3, pp. 335–359, Jul. 1970.

[34] A. H. Marcus and S. A. Rice, “Phase transitions in a confined quasi-two-dimensional colloid suspension,” *Physical Review E*, vol. 55, no. 1, p. 637, 1997.

[35] R. C. Ball and J. R. Melrose, “A simulation technique for many spheres in quasi-static motion under frame-invariant pair drag and Brownian forces,” *Physica A: Statistical Mechanics and its Applications*, vol. 247, no. 1–4, pp. 444–472, Dec. 1997.

[36] *Low Reynolds Number Hydrodynamics with Special Applications to Particlate Media*. Prentice-Hall, 1965.

[37] S. Kim and S. J. Karrila, *Microhydrodynamics: Principles and Selected Applications*. Courier Corporation, 2013.

[38] *MATLAB and Statistics Toolbox Release 2014a*. Natick, Massachusetts, United States: The Mathworks, Inc.

[39] R. A. Segalman, A. Hexemer, R. C. Hayward, and E. J. Kramer, “Ordering and Melting of Block Copolymer Spherical Domains in 2 and 3 Dimensions,” *Macromolecules*, vol. 36, no. 9, pp. 3272–3288, May 2003.

[40] P. Dillmann, G. Maret, and P. Keim, “Comparison of 2D melting criteria in a colloidal system,” *Journal of Physics: Condensed Matter*, vol. 24, no. 46, p. 464118, Nov. 2012.

[41] R.-J. Roe, *Methods of X-ray and Neutron Scattering in Polymer Science*. Oxford University Press, 2000.

[42] K. Dill and S. Bromberg, *Molecular Driving Forces: Statistical Thermodynamics in Biology, Chemistry, Physics, and Nanoscience*. Garland Science, 2010.

[43] P. C. Hiemenz and R. Rajagopalan, *Principles of Colloid and Surface Chemistry, Third Edition, Revised and Expanded*. CRC Press, 1997.

[44] D. Myers, *Surfaces, interfaces, and colloids: principles and applications*. Wiley-VCH, 1999.

[45] K. W. Kolasinski, *Surface Science: Foundations of Catalysis and Nanoscience*. John Wiley & Sons, 2008.

[46] M. Semmler, J. Rička, and M. Borkovec, “Diffusional deposition of colloidal particles: electrostatic interaction and size polydispersity effects,” *Colloids and Surfaces A: Physicochemical and Engineering Aspects*, vol. 165, no. 1, pp. 79–93, 2000.